EFFECT OF WELDING PARAMETERS ON THE SUSCEPTIBILITY TO HYDROGEN CRACKING IN LINE PIPE STEELS IN SOUR ENVIRONMENTS

A THESIS SUBMITTED TO
THE GRADUATE SCHOOL OF NATURAL AND APPLIED SCIENCES
OF
MIDDLE EAST TECHNICAL UNIVERSITY

BY

ÖZGÜR YAVAŞ

IN PARTIAL FULFILLMENT OF THE REQUIREMENTS
FOR
THE DEGREE OF MASTER OF SCIENCE
IN
METALLURGICAL AND MATERIALS ENGINEERING

DECEMBER 2006

Approval of the Graduate School of Natural and Applied Sciences

_____

Prof. Dr. Canan Özgen
Director

I certify that this thesis satisfies all the requirements as a thesis for the degree of Master of Science.

_____

Prof. Dr. Tayfur Öztürk
Head of Department

This is to certify that we have read this thesis and that in our opinion it is fully adequate, in scope and quality, as a thesis for the degree of Master of Science.

_____

Prof. Dr. Mustafa Doruk
Supervisor

Examining Committee Members

Prof. Dr. Tayfur Öztürk (METU, METE) _____

Prof. Dr. Mustafa Doruk (METU, METE) _____

Prof. Dr. Rıza Gürbüz (METU, METE) _____

Prof. Dr. Cevdet Kaynak (METU, METE) _____

Dr. Caner Batıgün (METU, METE) _____

I hereby declare that all information in this document has been obtained and presented in accordance with academic rules and ethical conduct. I also declare that, as required by these rules and conduct, I have fully cited and referenced all material and results that are not original to this work.

Name, Last name : Özgür Yavaş

Signature :

ABSTRACT

EFFECT OF WELDING PARAMETERS ON THE SUSCEPTIBILITY TO HYDROGEN CRACKING IN LINE PIPE STEELS IN SOUR ENVIRONMENTS

YAVAŞ, Özgür

M.S., Department of Metallurgical and Materials Engineering

Supervisor: Prof. Dr. Mustafa Doruk

December 2006, 66 pages

In this study, hydrogen induced cracking (HIC) behavior of welded steels used in petroleum lines under sour petroleum environments was investigated. The testing environment in NACE TM0284-2003 standard was used in order to simulate sour petroleum environment.

In order to investigate behavior of welding parameters, used in pipe production, on HIC, welds were done with different line energies. Two different API X-65 steels were used in welding operations. The specimens taken from welded zones were tested in testing environment. The specimens were examined metallographically. Crack lengths were measured with a computer program. The results obtained were discussed in view of metallurgical and welding parameters aspects.

The result obtained from this investigation led to a general conclusion that, the metallurgical parameters of steels used in pipe production were more important than welding parameters regarding their effect on HIC. It was shown that the composition and microstructural grain size of steels were in direct relation to HIC.

Key Words: Hydrogen induced cracking in sour petroleum environment, hydrogen cracks, corrosion of API X-65 steels.

ÖZ

EKŞİ PETROL ORTAMLARINDA KULLANILAN ÇELİKLERİN HİDROJEN ÇATLAMALARINA KARŞI HASSASİYETLERİNDE KAYNAK PARAMETRELERİNİN ETKİSİ

YAVAŞ, Özgür

Yüksek Lisans, Metalurji ve Malzeme Mühendisliği Bölümü
Tez Yöneticisi: Prof. Dr. Mustafa Doruk

Aralık 2006, 66 sayfa

Bu çalışmada petrol hatlarında kullanılan kaynaklı çeliklerin ekşi petrol ortamlarındaki hidrojen tetikli çatlama davranışları incelendi. Ekşi petrol ortamını simüle etmek için NACE TM0284-2003 standardındaki deney düzeneği kullanıldı.

Boruların üretimi esnasında kullanılan kaynak parametrelerinin hidrojen tetikli çatlamaya karşı davranışlarını incelemek amacıyla farklı ısı girdilerinde kaynaklar yapıldı. Kaynaklar için iki farklı API X-65 çeliği kullanıldı. Kaynaklı bölgelerden alınan numuneler deney düzeneğinde test edildi. Numuneler metalografik olarak incelendi. Çatlak boyları bilgisayar programı ile ölçüldü. Elde edilen sonuçlar metalurjik parametreler ve kaynak parametreleri açısından incelendi.

Bu araştırmadan elde edilen sonucu, boru üretiminde kullanılan çeliklerin metalurjik parametrelerinin hidrojen tetikli çatlama davranışlarına karşı etkisinin kaynak parametrelerinden daha önemli olduğu şeklinde genellemek mümkündür. Çeliklerin kimyasal kompozisyonları ve içyapı tane büyüklüklerinin hidrojen tetikli çatlama üzerinde doğrudan etkili olduğu gösterildi.

Anahtar Kelimeler: Ekşi petrol ortamlarında hidrojen tetikli çatlamalar, hidrojen çatlakları, API X-65 çeliklerin korozyonu.

TABLE OF CONTENTS

ABSTRACT iv
ÖZET vi
TABLE OF CONTENTS viii

1. INTRODUCTION 1

2. THEORY 3
2.1. Mechanisms of HIC in Steel 3
2.2. Effect of Environmental Variables on HIC in Steels 10
2.3. Effect of Metallurgical Variables on HIC in Steels 14
2.4. Submerged Arc Welding (SAW) 17
2.4.1. Fluxes for SAW 19
2.4.2. Electrodes and Filler Metal for SAW 20
2.4.3. Temperature Distributions During Welding 21
2.4.4. Cooling Rate After Welding 22

3. EXPERIMENTAL PROCEDURES 24
3.1. Materials 24
3.2. Experimental Facilities 25
3.3. Implementation of Tests 27

4. RESULTS 32
4.1. Macroscopic Examination 32
4.2. HIC Test Results 34
4.3. Microscopic Examination 35
4.4. Hardness Test Results 39
4.5. Impact Toughness Test Results 40

4.6. Chemical Analysis 41
4.7. SEM Analysis 42
4.8. Grain Size 42

5. DISCUSSION 43
5.1. Cracked Specimen Group Analysis 43
5.2. Effect of Metallurgical Variables 44
5.3. Effect of Hardness 45
5.4. Effect of Welding Parameters 47

6. CONCLUSIONS 48

REFERENCES 49

APPENDIX A: MICROGRAPHS OF CRACKED SPECIMENS 53
APPENDIX B: HARDNESS VALUES OF TEST SPECIMENS 64
APPENDIX C: CHEMICAL ANALYSIS OF TEST SPECIMENS 66

CHAPTERS

1. INTRODUCTION

Corrosive environments have always posed problems for the oil and gas industry.[1] Aggressive environments such as hydrogen sulfide, carbon dioxide, chloride, and sulfur compounds are encountered often in crude oil survey, oil and natural gas transportation, and storage of raw petroleum materials and products.[2]

Pipe lines are the most efficient facilities for the transportation of oil and gas. Line pipe steels used in sour service (containing H_2S) are prone to hydrogen induced cracking (HIC), also known as stepwise cracking (SWC), depending on metallurgical and environmental factors. The metallurgical factors consist of alloying elements, microstructure, strength, segregation, and the shape of non-metallic inclusions. Some of the environmental factors that can cause HIC are the partial pressures of hydrogen sulfide (H_2S) and carbon dioxide (CO_2), temperature, pH of the medium, moisture, and the presence of aggressive ions.[1]

Many failures of sour gas line pipes have occurred around the world as a result of HIC.[3] Considerable effort has been expended by steel line pipe producers, users, and research organizations seeking to understand the mechanism of HIC so that a laboratory test method can be developed to identify and quantify material susceptibility to HIC, which would allow for production of steels with greater resistance to HIC.[4]

NACE International has developed a standard test, TM-02-84, to evaluate the performance of the line pipe.[5] The method describes procedures for

evaluating the resistance of line pipe steels and weldments to stepwise cracking induced by hydrogen absorption aqueous sulfide corrosion.

In general, the relative H_2S susceptibility can be directly related to the steel microstructure and sour gas environment.[6] On the other hand, there have been published few data about relation between H_2S susceptibility and the production parameters of the line pipes.

The aim of this study is to identify the welding parameters of the line pipe that yield the highest resistance to sour environments. NACE International laboratory test method was applied to evaluate the susceptibility to cracking of welding and heat affected zone (HAZ). The submerged arc method was used for welding operation and in order to obtain different weldments, line energies were varied for all test specimens. The line pipe steels used in this investigation were API X-65 grades delivered by two different producers. The welded test specimens were sectioned, polished, and etched metallographically, if necessary, so that cracks could be distinguished from small inclusions, laminations, scratches, or discontinuities. Crack length and crack length ratio (CLR) were calculated for each section. Based on the generated data, it was tried to identify the welding parameters and the metallurgical variables that are expected to have a pronounced effect on the resistance of welded structures to HIC in sour environments.

2. THEORY

2.1. Mechanisms of HIC in Steel

Hydrogen induced corrosion is primarily an electrochemical reaction between metal and the sour aqueous environments. Hydrogen produced by corrosion readily dissolves and diffuses in metal crystals and can have dramatic effects on mechanical strength and ductility. In sour environments aqueous hydrogen sulfide, H_2S, accelerates hydrogen entry and hydrogen damage in steels. The S^{2-} anion slows (poisons) the recombination reaction,

$$H + H \longrightarrow H_2,$$

and provides a greater activity of nascent atomic hydrogen on the surface.[7] Even a reaction as simple as the hydrogen evolution reaction occurs in a number of consecutive steps. They are;

1) transport of hydrated proton to the double layer,
2) loss of the water of hydration shield in the vicinity of the double layer,
3) adsorption of the proton to the electrode surface,
4) discharge (electronation) of the proton to an adsorbed hydrogen atom,
5) a) chemical combination of two adjacent hydrogen adatoms to form a hydrogen molecule – possibility of surface migration between site of discharge and site of recombination,
   b) electrodic combination of an adatom and a proton to form a hydrogen molecule,
6) desorption of H_2, and
7) bubble formation as H_2 molecules coalesced, and evolution of bubbles.

This sequence is schematically illustrated in Figure 1.

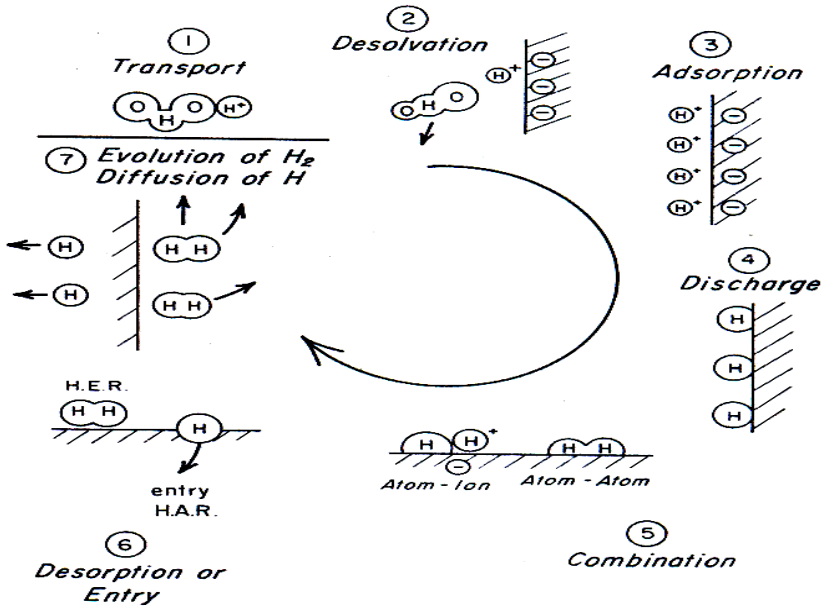

Figure 1. Processes of hydrogen evolution and absorption[8]

Two models for explaining hydrogen entry into the metal have been proposed. The first of these considers that the hydrogen enters in the same elementary form as it exists on the surface; that is, atomic or nascent hydrogen. In the second model hydrogen enters directly form a discharged proton (hydrogen ion) and does not pass through the intermediate absorbed phase. These models are schematically described in Figure 2.

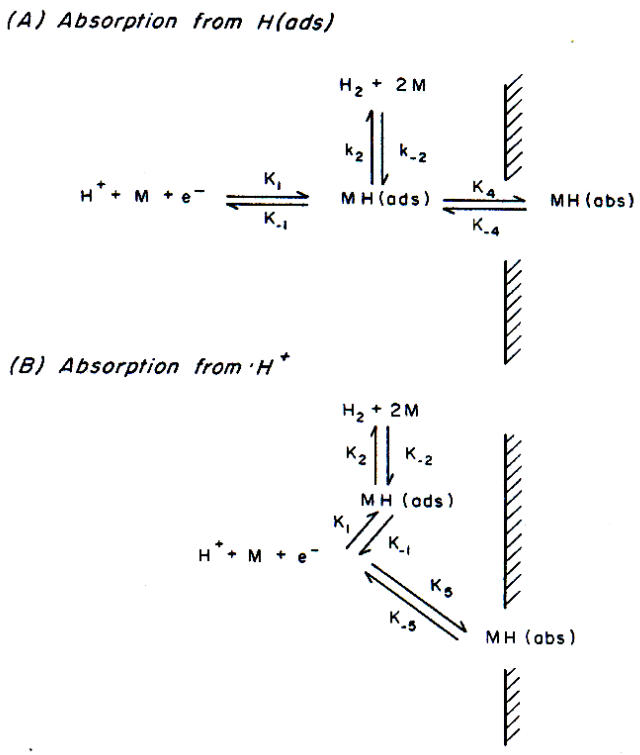

Figure 2. Models for hydrogen entry into metals[8]

In the first model the absorption step and chemical desorption (recombination) step are competing. The absorption step is written as a fast step meaning that equilibrium is attained rapidly and the step proceeds with little activation energy. In Figure 2 k's are the specific rate constants for the various steps. The subscripts 1 and -1 refer to the discharge step, and 4 and -4 to the absorption step. The chemical desorption step can be replaced by the electrodic desortion step (k3 and k-3 rate constants) if that mechanism occurs.

In the second model the hydrogen ion is discharged and passes immediately into the metal with no intermediates involved. In other words the hydrogen absorption reaction is competing for the same discharge protons as the hydrogen evolution reaction. The specific rate constant for the absorption step in this model is denoted by the subscript 5.

Two models for explaining hydrogen chemisorption that related to the two models of hydrogen entry have been proposed also (Figure 3). In first model, called r-type absorption, the hydrogen adatoms are outside the electronic cloud but immediately atop a corresponding metal atom. The distance of the metal-hydrogen bond is about 2,5 A. The bonding is largely covalent with the hydrogen being the slightly negative member of the dipole. In second model, called s-type absorption, the hydrogen adatom is partly within the electronic cloud of the metal. The hydrogen behaves more like a proton dissolved in the surface layer and the bonding is more ionic hydrogen being positive. This situation represents a higher energy state than r-type absorption but lattice defects and other surface imperfections significantly reduce the energy and favor s-type absorption.[8]

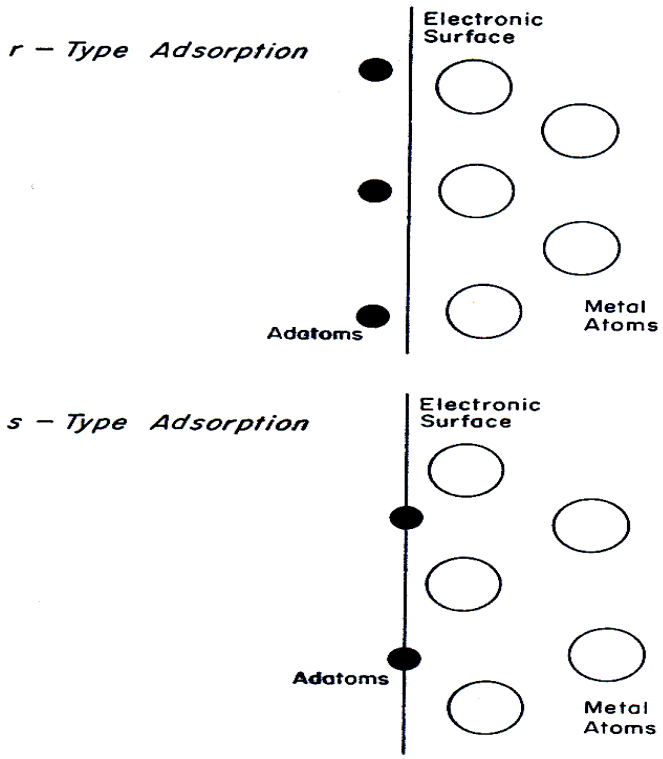

Figure 3. Models for chemisorbed hydrogen[8]

The absorption of hydrogen inside the cathode is preceded by its adsorption in atomic form on the metal surface. The permeation rate is proportional to the coverage of the metal surface by adsorbed hydrogen atoms, and this, in turn, is a function of the cathodic current density. Theoretically, a linear relationship between the permeability and the square root of cathodic current density can be expected. [9]

Hydrogen diffusing through a metal lattice accumulates at metallurgical inhomogeneities or traps. The accumulation causes a lag in the hydrogen flux through a sheet specimen of the metal. The difference between consecutive transients shows that hydrogen penetrates in a much shorter time after the traps have been filled.

A classification of traps is shown in Table 1. It is apparent that traps may result from solute atoms, dislocations, particle-matrix interfaces, grain boundaries, and internal voids or cracks. Because traps are associated with various microstructural features, alloying and metallurgical treatments to modify trapping properties offer a promising way to the development of alloys with maximum resistance to hydrogen damage. Deep or irreversible trapping reduces the population of hydrogen at the crack tip and often increases resistance to HIC. Conversely, shallow or more reversible traps permit more rapid hydrogen transport, which allows some traps to reach a critical concentration necessary to initiate cracking.[7]

Table1. Classification of hydrogen traps[7]

Trap Class	Example of trap	Interaction energy eV	Character if known	Influence Diameter, Di
Point	Ni	0.083	most probably reversible	a few interatomic spacing
	Mn	0.090		
	Cr	0.100		
	V	0.160		
	Ce	0.160	reversible	
	Nb	0.160		
	Ti	0.270		
	O (vacancy)	0.710	getting more irreversible	
	Ta (vacancy)	0.980		
	Ia (vacancy)	0.980		
	Nd (vacancy)	1.340		
Linear	Dislocations	0.310	reversible	3 nm for an edge dislocation
		0.250	reversible	
	Intersection of three grain boundaries	-	Depends on coherency	-
Planar or bidimensional	Particle/matrix interfaces			
	TIC	0.980	Irreversible, gets more reversible as the particle is more coherent	Diameter of the particle, or a little more as coherency increases
	Fe3C	0.800 – 0.980		
	MnS	-		
	Grain Boundaries	0.27	reversible	Same as dislocation reversible or irreversible
	Twins	-	reversible	a few interatomic spacing
	Internal surfaces	-	-	-
Volume	Voids	> 0.220	-	Dimension of the defect
	Cracks	-	-	
	Particles	-	Depends on exothermicity of the dissolution of H by the particle	

After hydrogen entry to the metal, sufficient hydrogen builds up at crystalline or metallurgical inhomogeneties, atomic or nascent hydrogen will recombine to form molecular H_2. Accumulated molecules nucleate the gas phase, which develops very high pressures sufficient to rupture interatomic bonds, forming

microscopic voids and macroscopic blisters.[7] The effective pressure built up within steel specimens by precipitating hydrogen, and the pressure necessary to produce microcracks and blisters.[9] The blisters will embrittle the lattice and generally degrade mechanical properties.[7]

The surface adsorption explains the hydrogen entry to the steel by decreasing the surface free energy of the metal or lowering cohesive energy of the metal. The surface free energy, γ, of a metal is lowered by the adsorption of hydrogen upon the surface of a crack, and that therefore the fracture stress, is thereby lowered. The lowering of the surface free energy means that the work needed reversibly to break the cohesive bonds across a crystallographic plane of the two-component lattice, one component of which is mobile at the temperature in question, is less than that required for the similar operation on the corresponding pure metal. However, in this explanation the mechanistic path is not specified.

The decohesion theory explains mechanistic point of view of HIC. The decohesion theory of hydrogen induced crack propagation utilizes a stress criterion, postulating that dissolved hydrogen in iron at a sufficiently large concentration decreases the maximum cohesive force between the iron atoms. The shape of the cohesive force-distance curve is shown in Figure 4. That the area under this curve is smaller when iron is in equilibrium with hydrogen than in the absence of hydrogen is a thermodynamically necessary consequence of the lowering of γ by hydrogen. [10]

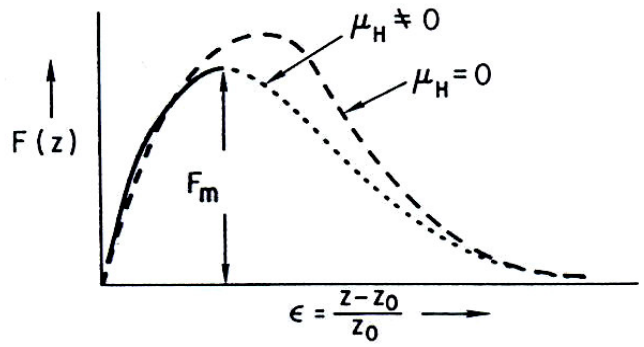

Figure 4. The hypothesized course of the cohesive force-strain curve when in equilibrium with hydrogen in the environment. In the absence of hydrogen, the cohesive force across a given crystallographic plane follows the dashed curve as a function of interatomic spacing[10]

2.2. Effect of Environmental Variables on HIC in Steels

The phenomenon of HIC was explained by hydrogen entry to the steel in trap points and, blistering and cracking caused by this hydrogen entry. The entry of hydrogen and crack propagation is affected by environmental variables and metallurgical variables. Hydrogen permeability is primarily affected by pH, H2S concentration, H2S - CO2 environments and temperature. These variables are explained below;

- pH and H_2S Concentration

Hydrogen permeability in steel ($[Per_{Fe}]$) is formulated as a function of P_{H2S} and pH;

$$([Per_{Fe}]) = 7,1 + 0,96 \times (1,4 \log P_{H2S} - 0,51\ pH),$$

where $0,1\ MPa \geq P_{H2S} \geq 1 \times 10^{-3}$ MPa and $pH \leq 5$;

$$([Per_{Fe}]) = 3,3 + 0,75 \times (0,3 \log P_{H2S} - 0,51\ pH),$$

where $10^{-3}\ MPa > P_{H2S} \geq 10^{-5}$ MPa and $pH \leq 5$.

Figure 5 shows the dependence of [Per_{Fe}] on P_{H2S} and pH. [Per_{Fe}] increases with an increase in P_{H2S} and is proportional to the logarithm of P_{H2S} with the slope of 0,3 in the range from 1 x 10^{-5} to 1 x 10^{-3} MPa. [Per_{Fe}] is proportional to the logarithm of P_{H2S} with the slope of 1,4 in the range from 1 x 10^{-3} to 0,1 MPa. [Per_{Fe}] also increases with a decrease in pH and is proportional to pH with the slope of -0,51 in the range from 3 to 5. [11]

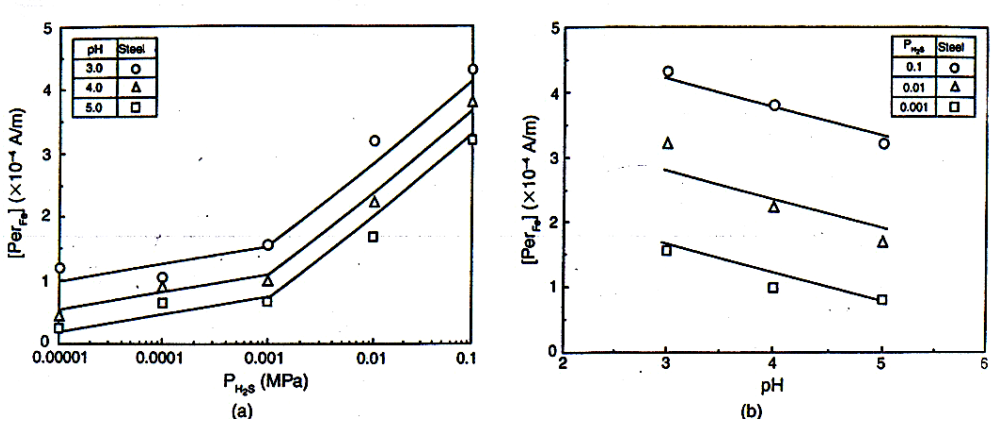

Figure 5. Effect of P_{H2S} and pH on [Per_{Fe}] [11]

In summary, cracking tends to increase with decreased pH and H_2S is predictably more effective in causing cracking at higher H_2S concentrations.[12]

- H_2S - CO_2 Environments

The effect of the partial pressure of H_2S (P_{H2S}) on the permeation rate in the case of P_{CO2} = 10 atm is shown in Figure 6. The maximum values of permeation rate increase with increasing P_{H2S}, but in case of P_{H2S} = 15 atm, the value of the permeation rate is lower than that in the case of P_{H2S} = 5atm. The permeation rates at P_{H2S} = 5 and 15 atm, increases with time to reach maximum values and then decreases to the steady state. On the other hand, the permeation rates at P_{H2S} = 0,15, 1 and 2 atm increase with time and reach a larger steady state value.

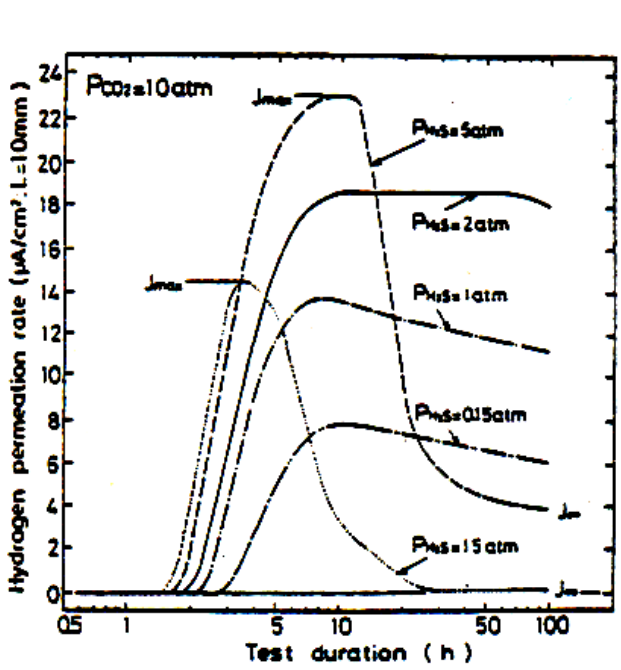

Figure 6. Changes of hydrogen permeation rate (P_{CO2} = 10 atm) [11]

Figure 7 shows the effect of P_{C02} on the permeation rate in the case of P_{H2S} = 2 atm , indicating that the values of the steady state permeation rate increase with an increase of the partial pressure of CO_2.

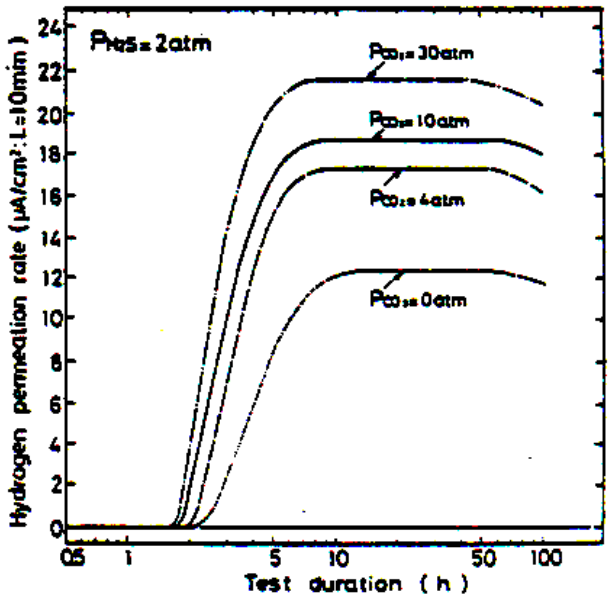

Figure 7. Changes of hydrogen permeation rate (P_{H2S} = 2 atm) [11]

Hydrogen entering into steel is generated by corrosion at the steel surface. The effect of the partial pressure of H_2S and CO_2 on the corrosion rate is mapped out in Figure 8. There are two areas with high corrosion rate: The area in which P_{CO2} is high and P_{H2S} is below 0,1 atm and the other one is the area in which P_{CO2} is high and P_{H2S} is between 1 and 5 atm, with the latter corresponding to the peak cracking area.

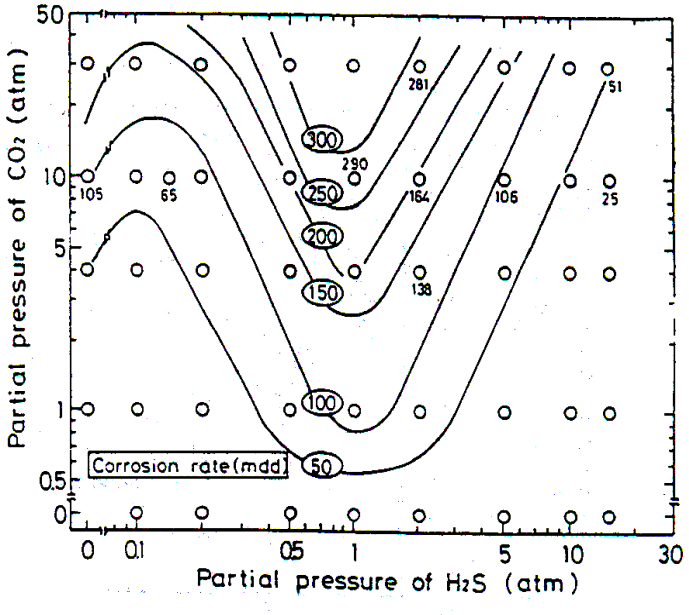

Figure 8. Corrosion rate in various H_2S and CO_2 partial pressure[11]

As mentioned above, the severest environment in the synthetic seawater, is the area in which P_{CO2} is high and P_{H2S} is between 1 and 5 atm. It is apparent that the higher H_2S pressure area (P_{H2S} > 5 atm) is a mild environment for HIC.[12]

- Temperature

The hydrogen permeation rate is considerably influenced by temperature as shown in Figure 9. The maximum value of the permeation rate at 25℃ is nearly equal to its steady state value. With increasing temperature, the hydrogen permeation rate decreases quickly, and the steady state is established at very low values. [12]

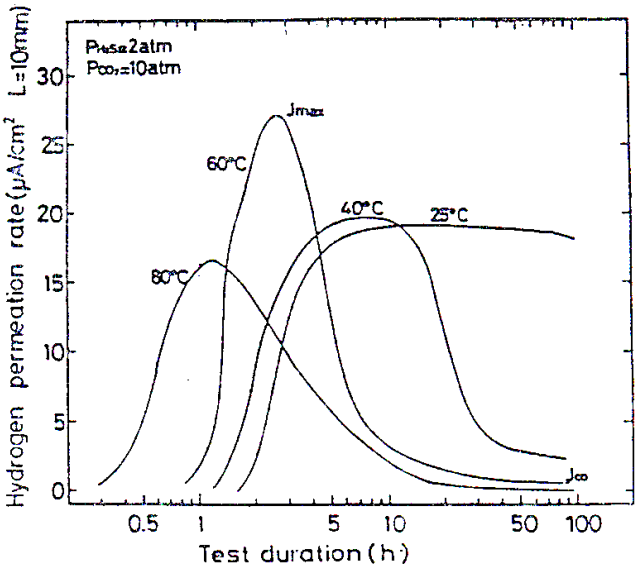

Figure 9. Effect of temperature on hydrogen permeation rate[11]

2.3. Effect of Metallurgical Variables on HIC in Steel

HIC susceptibility of line pipe steels is mainly affected by chemical composition, microstructure, and thermal history of the steel.

Manganese Sulfides: HIC resistivity of steels is mainly affected by MnS inclusions. HIC initiates at elongated Type II MnS inclusions. The association of HIC with MnS inclusions has led to attempts to decrease the HIC by lowering the inclusion content. One method of achieving this has been to reduce the levels of sulfur and oxygen. Inclusions with sharp edges and large surfaces are the preferred sites for initiation of HIC. The geometrical shape of inclusions is considered to play a more important role than the chemical composition. The susceptibility of line pipe steel to HIC can be reduced by means of inclusion-shape control.[13]

Deoxidation Practice: The fully killed steels are more susceptible to cracking than the semi-killed steels. Reason of this is increasing deoxidation leads to a higher solubility of sulfur in the melt, and can convert ellipsoidal Type I MnS

to elongated, stringer-like Type II MnS in the rolled product, leading to higher cracking susceptibility.[13,14]

Controlled Rolling: The deformability of MnS increases with decreasing temperature, and thus, controlled rolling is conducive to the formation of the elongated Type II MnS stringers that provide preferred sites for the initiation of HIC.[14]

Anomalous Microstructure: The anomalous structures would be prone to hydrogen embrittlement.[15,16,17]

Heat Treatments: Heat treatments can reduce the susceptibility of steels to HIC.[16,18]

Casting Practice: The susceptibility of steels to HIC depends on sampling location in casting. Generally, HIC is greatest at the most highly segregated parts. But no definite differences in HIC resistance attributable to the casting mode, including both continuously cast and ingot cast.[15,19,20]

Strength of the Steel: Susceptibility to HIC increases with increasing strength for steels with tensile strengths above 690 MPa. But in commercial line pipe steels, other factors such as non-metallic inclusions and anomalous microstructures are more significant than strength. [21]

Stresses: Internal stresses help the formation of microcracks that behave like a trap point and increase the absorption of H atoms. [21] When steel specimens under tensile stress are exposed to H_2S environments, internal cracks or blisters are often observed. These tend to be oriented in the rolling direction of the steel and may be linked by transverse cracks-characteristics resembling those observed in HIC tests on unstressed specimens. Therefore, externally applied stresses may decrease the HIC resistance of steel.[17, 21, 22]

Weldments: There have been some different theories about the behavior of welds and HAZ under sour environments. According to one of the theories the sour gas pipeline failures by HIC were always located near spiral welds but never connected with weld defects of any kind. In laboratory tests of line pipe steels from a number of sources HIC was never observed in welds or in the HAZ of welds.[9] However, the other theory reported that weld metal, with its dendritic microstructure and oxide inclusions dispersed in the form of fine globules, has excellent resistance to HIC.[16] However according to another view the welds are dangerous because they can cause straight internal cracks to be convened to the stepwise form.[23] In summary, the behavior of the weldments under sour environments has not just been understood clearly.

Alloying Elements:

Copper: Cu addition causes to develop a protective film on steel surface in sour environments which results in reduction of corrosion and hydrogen absorption rate. Cu also accelerates the recombination of hydrogen atoms and thus decreases the hydrogen activity. Cu additions increase the HIC resistivity of steels. [15, 16, 18, 21]

Niobium: Nb addition retards the recrystallization of austenite and increases the nucleation sites together with nucleation rates during ferrite transformation. This resulted in decrease of ferrite grain size but increase in deformation resistance of γ phase. As this causes more elongated inclusions especially MnS, Nb additions decrease the HIC resistivity of steels. [24, 25, 26]

Chromium and Molybdenum: Adding Cr and Mo increase the hardenability and promote the low temperature transformation products with more traps for HIC. Therefore, Cr and Mo additions decrease the HIC resistivity of steels.[5, 26]

2.4. Submerged Arc Welding (SAW)

The use of automated welding processes is the present trend in the fabrication industries to obtain high production rates and high precision. Because of its high reliability, deep penetration, capability to weld thicker sections, prevention of atmospheric contamination of weld pool, smooth finish and high productivity, SAW has become a natural choice in industries for fabrication, especially for welding of pipes. With the growing emphasis on the use of automated welding systems, SAW is employed in semiautomatic or automatic mode in industry. In such automated applications, a precise means of selection of the process variables and control of weld bead shape has become essential because mechanical strength of welds is influenced not only by the composition of the metal, but also by the weld bead shape. The weld bead shape is an indication of bead geometry. The acceptable or appropriate weld bead shape depends on factors such as line power which is the heat energy supplied by the arc to the base plate per unit length of weld, welding speed and joint preparation.[27, 28]

SAW involves formation of an arc between a continuously-fed bare wire electrode and the workpiece. The process uses a flux to generate protective gases and slag, and to add alloying elements to the weld pool. A shielding gas is not required. Prior to welding, a thin layer of flux powder is placed on the workpiece surface. The arc moves along the joint line and as it does so, excess flux is recycled via a hopper. Remaining fused slag layers can be easily removed after welding. As the arc is completely covered by the flux layer, heat loss is extremely low. This produces a thermal efficiency as high as 60% (compared with 25% for manual metal arc).[29] There is no visible arc light, welding is spatter-free and there is no need for fume extraction. Figure 10 illustrates the SAW process in rudimentary form, but after four decades of development and use there are a number of variations in arrangement of electrodes and sources of filler metal. The user, and his exactness in carrying out the details of SAW procedures probably exerts more influence on the

final outcome of welding than is the case with any other arc welding process.[30]

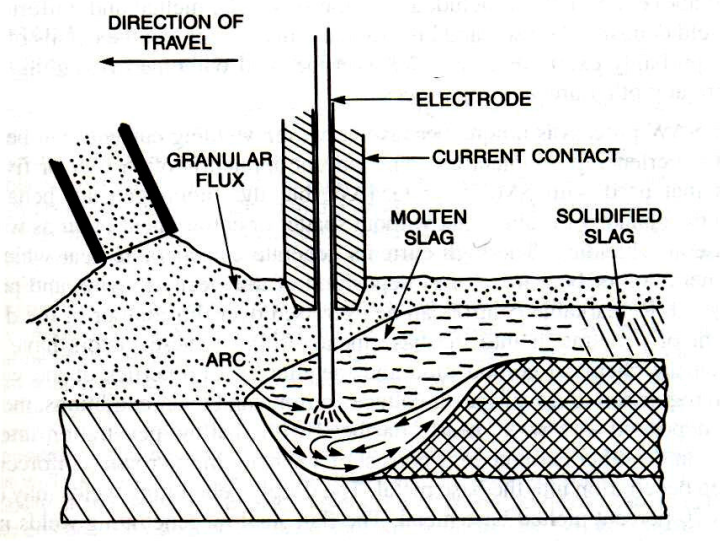

Figure 10. Diagrammatic sketch of the submerged arc welding process[30]

Current for SAW can be either dc or ac. Welding is most conveniently performed in the flat position, although some SAW application is done in the horizontal position. Vertical and overhead deposition is impracticable because of the high fluidity of the molten flux and weld metal. Some form of backing is required to prevent fall through of the weld metal from a completely penetrated joint. Multiple electrodes can be used in various arrangements to deposit weld metal more rapidly or to surface an area. The electrodes may be positioned side-by-side, or in tandem, and their arcs can be grounded through the base metal, or between electrodes via the weld pool. Some use has been made of flat strip as the consumable electrode when employing SAW for surfacing. Sometimes a supplementary filler metal - either solid or tubular powder filled - is fed into the arc to increase the rate of metal deposition.[30]

2.4.1. Fluxes for SAW

Fluxes that are used to form the protective molten shield for the SAW arc and to cover the weld metal are acid, neutral, or basic in nature. Their composition and functions actually are more complex and demanding than those used in steel melting because they must accomplish proper venting, shielding, alloying, removal of solidified flux, etc., while welding is in progress. Of course, no change can be made in the flux applied during the SAW operation (as is often the practice in steelmaking). Even the size of granular flux particles and the height of the unmelted flux burden above the molten flux and weld metal are important in allowing gases to escape and to assist in contouring the top surface of the weld bead.[30]

Fluxes used in SAW are granular fusible minerals containing oxides of manganese, silicon, titanium, aluminum, calcium, zirconium, magnesium and other compounds such as calcium fluoride. The flux is specially formulated to be compatible with a given electrode wire type so that the combination of flux and wire yields desired mechanical properties. All fluxes react with the weld pool to produce the weld metal chemical composition and mechanical properties. It is common practice to refer to fluxes as 'active' if they add manganese and silicon to the weld, the amount of manganese and silicon added is influenced by the arc voltage and the welding current level. The main types of flux for SAW are:

- **Bonded fluxes** - produced by drying the ingredients, then bonding them with a low melting point compound such as a sodium silicate. Most bonded fluxes contain metallic deoxidizers which help to prevent weld porosity. These fluxes are effective over rust and mill scale.
- **Fused fluxes** - produced by mixing the ingredients, then melting them in an electric furnace to form a chemically homogeneous product, cooled and ground to the required particle size. Smooth stable arcs, with welding currents up to 2000A and consistent weld metal properties, are the main attraction of these fluxes.[29]

As a rough rule, the amount of flux melted during the SAW operation will be equal to the weight of the electrode deposited. However, this relationship depends on the composition of the flux and the welding conditions. For example, the welding voltage affects the amount of flux melted. Longer arc lengths which accompany higher welding voltages can impart more heat to the flux than shorter arcs. Therefore, if an alloy containing flux is being used to contribute to the composition of the weld metal, the welding conditions (particularly the voltage or arc length) must be carefully controlled to maintain a uniform flux-to-metal melting ratio and thus ensure consistent chemical composition along the length of the weld.[30]

2.4.2. Electrodes and Filler Metal for SAW

Most carbon steel SAW electrodes are solid round wire because this is the lowest-cost form, but certain steels are available as coils of tubular composite electrodes. The composite form permits manufacture of small quantities, and the composition (especially for low-alloy steel SAW electrodes) can be set precisely through the metal powders included in the core. This kind of electrode can be made on the same production facilities used for flux cored electrodes. Although solid wire electrodes and composite electrodes may be interchangeable from a chemical-composition standpoint, they require different welding parameters to produce a given size and shape of weld. Under the same welding conditions, composite electrodes produce a sound, homogenous weld metal, but penetration usually is less than achieved with a solid wire electrode.[30]

Weld metal produced by SAW is clean and sound because of the excellent protection afforded by the blanket of molten slag, the deoxidation that can be effectively arranged via electrode or flux composition, and the relatively hot, fluid weld pool that allows gases and impurities to escape from the molten metal. SAW also can function as a low-hydrogen process, unless the flux has been contaminated with moisture or the wire has been contaminated with

hydrogenous compounds (e.g., soap, oil, grease). However, problems can arise in SAW with hot cracking, coarse grain microstructure, and segregation as a result of the relatively slow solidification of a large mass of molten metal.[30]

2.4.3. Temperature Distributions During Welding

The temperature distribution during welding operations is in almost continual change as the work pieces are heated and cooled, until the entire weldment cools to ambient temperature. It is this dynamic behavior which makes graphic presentation of welding temperature distribution so difficult. A quasi-stationary portrayal is employed for Figures 11, and this is commonly practiced. Diagrams of this kind show an instantaneous distribution of temperatures at a specified time in the course of welding - usually at the moment peak temperature is reached in the heat-affected base metal immediately adjacent to the weld. As the heat source continues to travel, and as heat is conducted to cooler areas, the temperature distribution changes as dictated by a number of conditions. The extent of superheating in the weld zone and the thermal conductivity of the solid base metal play a part in establishing the distribution of temperature at each point in time. [30]

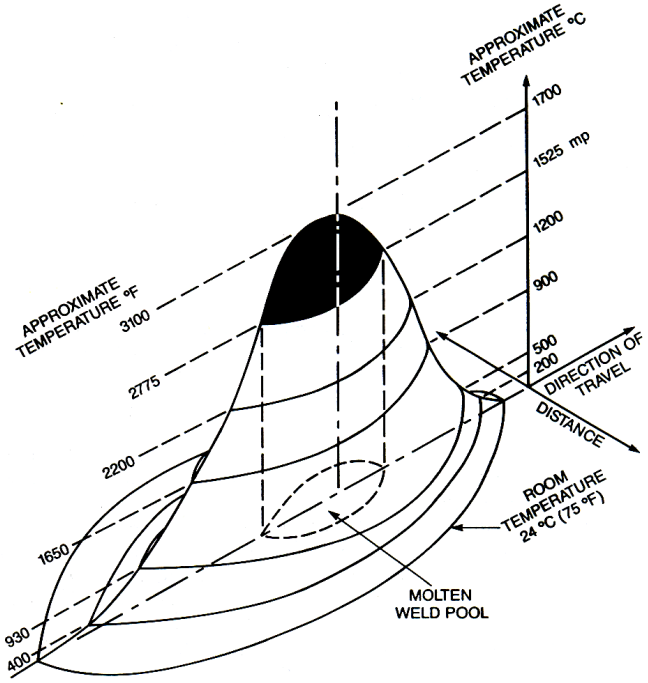

Figure 11. Schematic illustration of quasi-stationary surface temperature profile produced by a welding heat source moving at medium travel speed across a steel plate[30]

2.4.4. Cooling Rate After Welding

Cooling is complex because many more features of a weldment and welding procedure exert an influence, and because the rate of cooling has a dominating effect on the final microstructure and properties. Three general features have a profound influence on the cooling rates at various locations in a weldment;

(1) the weld zone, or nugget, which serves as a heat source during the course of the welding process;
(2) the mass of base metal, along with any intimately contacting metal fixtures that can provide a heat sink; and
(3) the initial temperature of the base metal and fixtures.

Hardness testing has been proposed as a practical indicator for HAZ cooling rate because a given steel when continuously cooled at various rates from above its critical range will transform to particular microstructures each having intrinsic levels of hardness; that is, both the microstructure and its hardness are firmly determined by the rate of continuous cooling that prevails as the austenitized steel undergoes transformation. In general, faster cooling rates produce harder microstructure (up to the maximum obtainable hardness for each steel). [30]

3. EXPERIMENTAL PROCEDURES

3.1. Materials

The testing materials are high strength low alloy line pipe steels. The grade of steels are complies with API 5L X-65. Totally three different steels are used for the experiments, that are shown in Table 2.

Table 2. Steels tested

No	Producer	Steel Grade	Wall Thickness	No of Coil	Heat Number
1	Manuf1	API 5L X-65	11.90 mm.	1,5E+10	513506
2	Manuf2	API 5L X-65	11.91 mm.	854051	730316664
3	Manuf2	API 5L X-65	14.27 mm.	723030	730323568

The chemical composition of the steels is given in Table 3. The carbon equivalent values in the table are calculated from following formula;

$$CE = \%C + \%Mn/6 + \%Ni/15 + \%Cr/5 + \%Mo/4 + \%Cu/13$$

Table 3. Chemical analysis of steels

Material	%C	%Si	%Mn	%P	%S	%Ni	%Cr	%Mo	%Cu	%Al	%Nb	CE
Manuf1 11,90 mm.	0.094	0.196	1.557	0.015	0.008	0.031	0.025	0.115	0.036	0.044	0.052	0.392
Manuf2 11,91 mm.	0.040	0.179	1.052	0.011	0.001	0.173	0.020	0.000	0.017	0.033	0.060	0.232
Manuf2 14,27 mm.	0.040	0.190	1.041	0.011	0.001	0.219	0.020	0.000	0.014	0.034	0.059	0.233

The mechanical properties of steels can be seen in Table 4 compared to the minimum required values according to API 5L for X-65 grade.

Table 4. Mechanical properties of steels

Material	Yield Strength (N/mm^2)	Tensile Strength (N/mm^2)	Elongation (%)
Manuf1 11,90 mm.	487	576	34.4
Manuf2 11,91 mm.	498	575	35.9
Manuf2 14,27 mm.	503	578	35.4
API 5L X-65	min. 448	min. 531	min.%23

3.2. Experimental Facilities

In this study the following instruments were used;

- Stero Microscope,
- Metal Microscope,
- Universal Hardness Test Machine,
- Optical Emission Chemical Analyzer,
- pH Meter,
- Thermometer,
- Flow meter.

A portable submerged arc welding machine was used to do the welds with different line energies. Potential difference and current together with welding speed of the machine can be controlled to obtain a high quality weld. Welding wire and flux used in welding procedure were fed manually. The speed of welding wire was automatically adjusted under each level of indicated in Table 5.

Table 5. Melt off rates of welding wire

Diameter (mm)	Melt Off	200 A	300 A	400 A	500 A	600 A	700 A	800 A	900 A	1000 A
1,6	cm / min	249	419	638	937					
	kg / h	2.31	3.90	5.94	8.71					
2	cm / min	127	213	312	460					
	kg / h	1.86	3.08	4.54	6.67					
2,4	cm / min		145	208	285	381				
	kg / h		3.04	4.35	5.94	7.98				
3,2	cm / min		69	102	140	180	229	285		
	kg / h		2.54	3.76	5.22	6.71	8.53	10.57		
4	cm / min			61	86	114	142	173	206	243
	kg / h			3.54	5.04	6.67	8.26	10.03	11.98	14.10
4,8	cm / min				56	74	94	114	135	158
	kg / h				4.67	6.17	7.85	9.57	11.25	13.20
5,6	cm / min					53	66	79	91	107
	kg / h					6.08	7.53	8.98	10.43	12.16

To simulate the sour environment, the HIC test apparatus according to NACE TM 0284 was used. In this test the sour environment is produced by employing 99,95 % H_2S gas in closed system. Figure 12 shows a schematic representation of the test system.

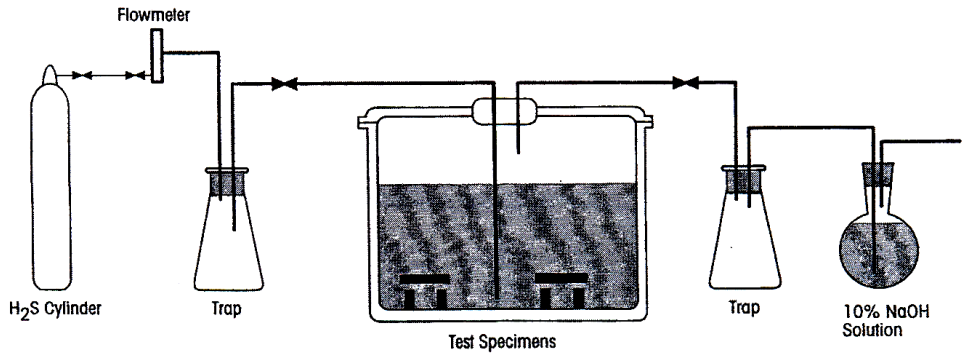

Figure 12. Schematic diagram of typical test system[5]

3.3. Implementation of Tests

- Line Energies

Nine different line energies were chosen, to cover a sufficiently wide range of combination of weld speed, voltage and current. Line energies were calculated from the following formula by 90 percent efficiency;

$$\text{Line Energy (kj / cm)} = \frac{0{,}9 \times 60 \times \text{Volt (V)} \times \text{Current (A)}}{\text{weld speed (cm / min)}}$$

The same line energy values were applied for three different steel groups. It is noted that the weld speed, voltage, and current values were different for the same line energies because they depend on the wall thickness of sheets. The weld parameters applied to test materials are summarized in Tables 6,7 and 8.

Table 6. Weld parameters for Manuf1 API 5L X-65 11,90 mm.

API 5L X-65 / 11.90 mm				
Parameter	**Weld Speed (cm / min)**	**Voltage (V)**	**Current (A)**	**Line Energy (kj / cm)**
1	270	800	30	4.77
2	240	800	30	5.40
3	200	800	30	6.48
4	90	400	30	7.20
5	80	400	30	8.10
6	70	400	30	9.27
7	50	300	30	9.72
8	45	300	30	10.80
9	40	300	30	12.15

Table 7. Weld parameters for Manuf2 API 5L X-65 11,91 mm.

API 5L X-65 / 11.91 mm				
Parameter	**Weld Speed (cm / min)**	**Voltage (V)**	**Current (A)**	**Line Energy (kj / cm)**
10	200	600	30	4.86
11	180	600	30	5.40
12	155	600	30	6.30
13	90	400	30	7.20
14	80	400	30	8.10
15	70	400	30	9.27
16	50	300	30	9.72
17	45	300	30	10.80
18	40	300	30	12.15

Table 8. Weld parameters for Manuf2 API 5L X-65 14,27 mm.

API 5L X-65 / 14.27 mm				
Parameter	**Weld Speed (cm / min)**	**Voltage (V)**	**Current (A)**	**Line Energy (kj / cm)**
19	270	800	30	4.77
20	240	800	30	5.40
21	200	800	30	6.48
22	180	800	30	7.20
23	120	600	30	8.10
24	100	600	30	9.72
25	65	400	30	9.99
26	60	400	30	10.80
27	55	400	30	11.79

- Test Specimens

Test specimens were prepared by using machining. The dimensions of the test piece were 350 x 1500 mm with a longitudinal nick, 7 mm deep and 60° flank angle. In all welding operations with different line energies, these nicks with the same geometry and dimensions were filled with weld. A view of these specimens is shown in Figure 13.

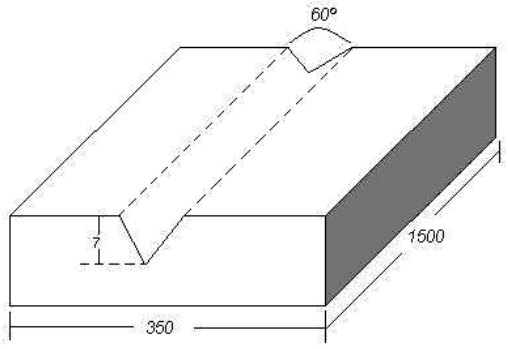

Figure 13. Design of welding specimens (All dimensions in mm).

- Welding Procedure

Lincoln P223 weld flux and 3,2 diameter S2MoTiB weld wire were used for all welding procedure. While the line energies were changed for each test specimen, all other parameters (the quality of weld, weld flux, weld wire, weld wire diameter and free wire length) were kept constant. In line of this approach, altogether 27 specimens were prepared for further examinations.

- The Hydrogen Cracking Sensitivity Test

Specimen Preparation: For each test, two coupons were taken from the material to be tested and one coupon was cut containing a weld. The shape of the coupons has been standardized as a rectangle 20 x 100 mm. The top and bottom faces were lightly machined until they are flat. The cut coupons were ground on a wet endless belt, and finish ground on dry 320 grit silicon carbide papers. The specimens were then degreased in acetone and handled with clean gloves.

Standard Test Solution: Synthetic sea water was chosen for the test solution. This solution was prepared in accordance with the requirements of ASTM D1141-52. The initial pH of the solution was 8.2.

HIC Test Procedure: Test solution was deaerated in a closed container by bubbling nitrogen through it at a rate of 100 ml/minute for one hour. The specimens were then placed horizontally in the solution with their wide faces vertical and their narrow faces horizontal. The lower face was raised from the cell bottom on bars of glass. The specimens were placed in the solution quickly in order to prevent oxygen pickup. The solution was then saturated by bubbling H_2S of 99,5 vol% purity at the rate of 200 ml/minute for one hour through an open ended tube with a 5 mm internal diameter. After one hour, the rate of purging decreased to 5 ml/minute to maintain a small positive pressure of H_2S in the test cell by the use of an outlet trap to prevent oxygen contamination from the air for 96 hours. The pH of the solution at the end of the test was 4,2. At the same time, the H_2S concentration in the solution was determined by idiometric titration and the result was 2500 ppm.

After purging, the specimen was removed from the solution, washed in running water, wire brushed to remove loose deposits, washed in acetone and dried in petroleum ether and cold air. Test specimens were sectioned transversely at three points. The intention of the sectioning procedures is to examine for cracks on a plane transverse to the rolling direction.

Metallographic Examinations: The sections obtained from test specimens were mounted in epoxy resin and polished stepwise. The steps were 360, 600, 800, 1000 grit grinding on SiC paper and polishing with 6 micron and 1 micron alumina silicate. Etching was done by 3 % Nital solution. Cracking was then examined by eye, and by microscopicically at magnifications of 100X. For each crack observed, the length of stepwise propagation is determined by using a computer program. Sections containing cracks were photographed showing the complete transverse sections with cracking. And also in order to see the weld quality, macro graphic examination of the welds was done with 360 and 1000 grit SiC grinding and etching by 10 % Nital solution.

Chemical Compositions: Chemical analysis of the steels was done by using optical emission chemical analyzer. Before doing test, the analyzer was calibrated with reference calibration block.

Mechanical Tests: Hardness levels of the welds, HAZ, and materials were determined by universal hardness testing machine. In each area, three measurements were done according to ASTM A370 standard. The points of measurement are shown Figure 14.

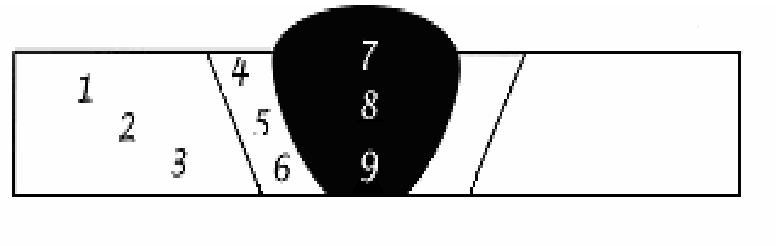

Figure 14. Hardness measurement points

Impact toughness values of the welds were determined at 0℃ by using an impact test machine. For each weld, three different tests were performed.

SEM Analysis: SEM analysis of the cracked samples was done in Metallurgical and Material Engineering Department at METU by using scanning electron microscope.

4. RESULTS

4.1. Macroscopic Examination

In Figure 15, the macro views of the welds for all three different steel groups at 2,5X magnification are given to indicate the quality of the welds, together with the geometry of the weld and HAZ.

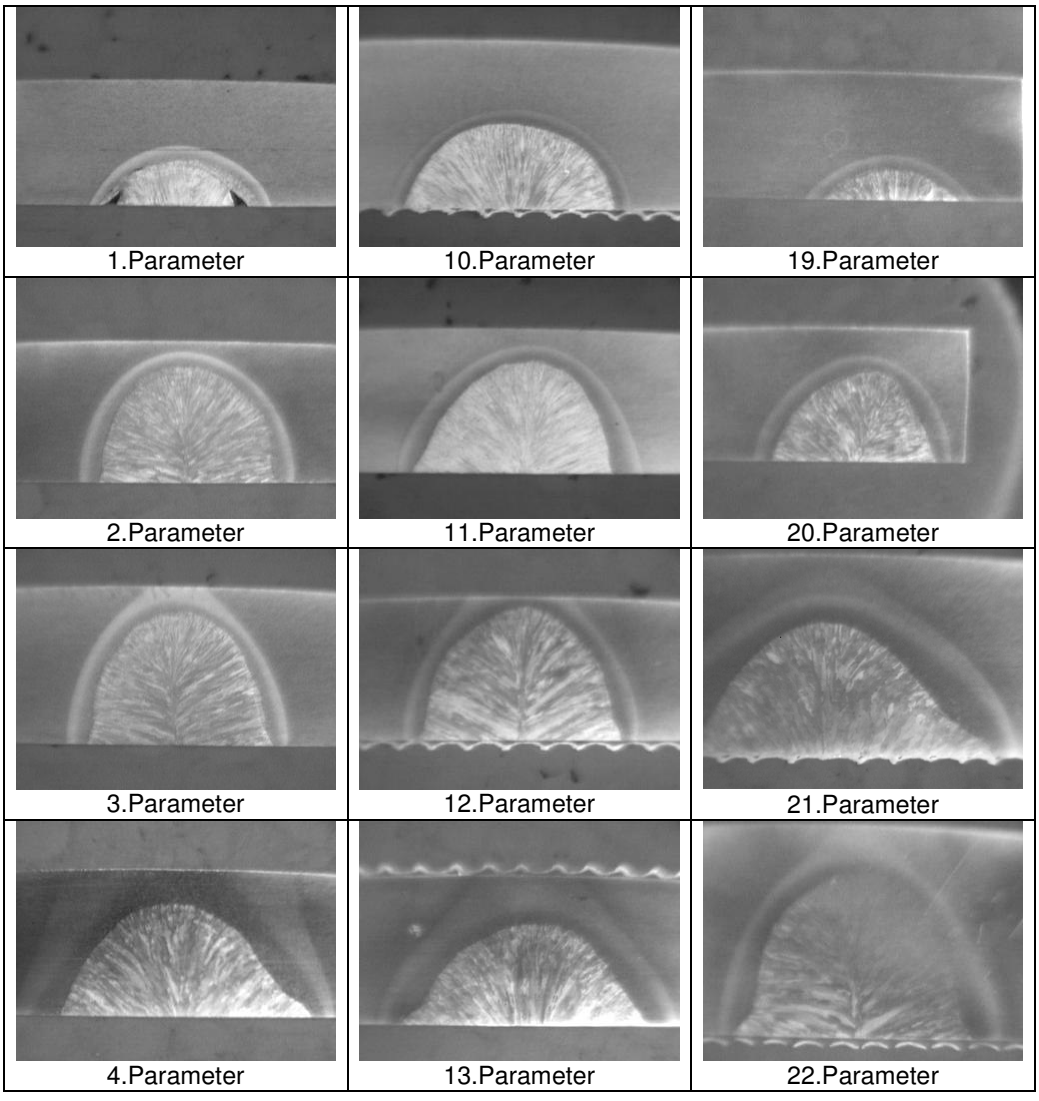

Figure 15. Macro photos of welds at 2,5X magnification

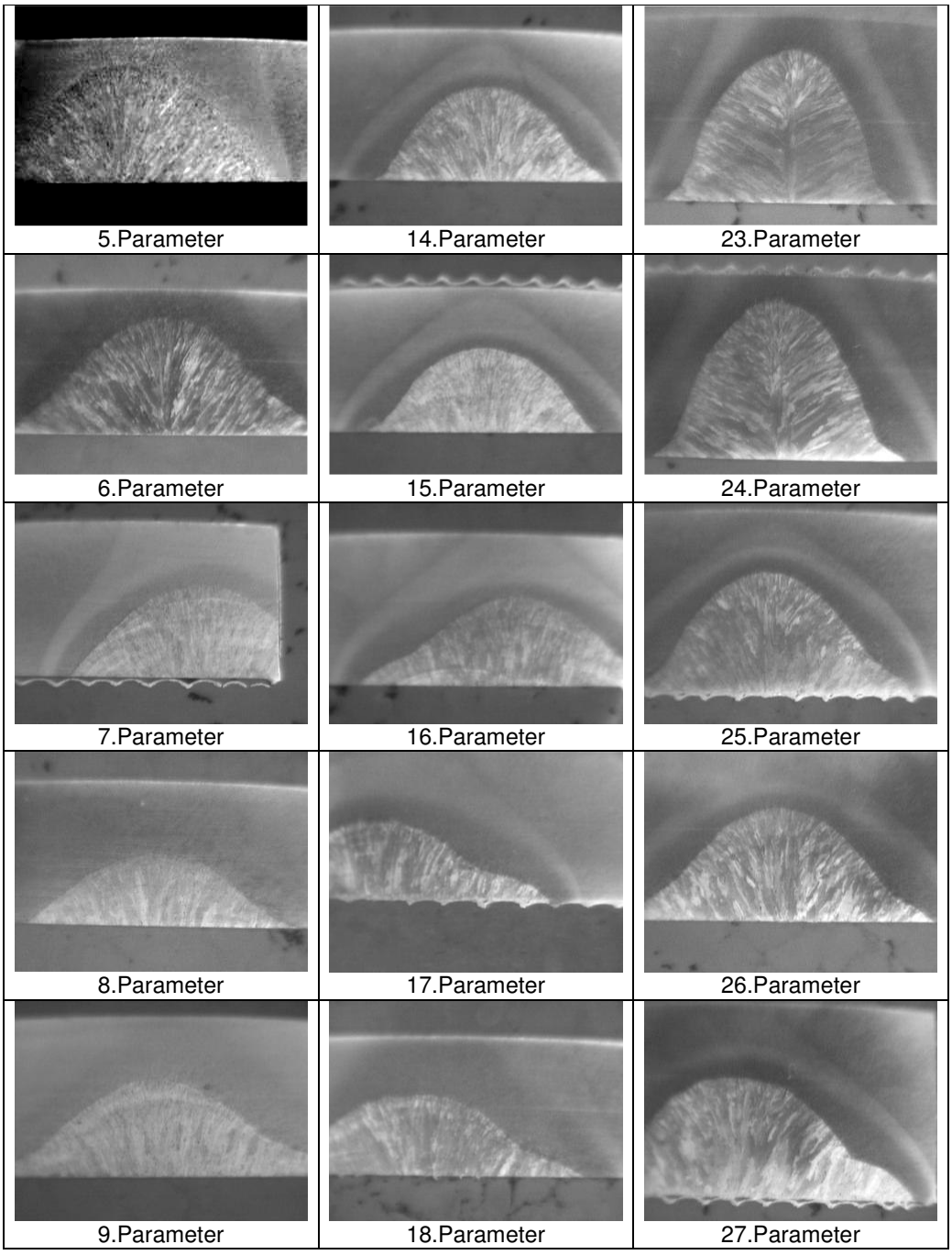

Figure 15 (continued)

4.2. HIC Test Results

HIC test results are shown in Tables 9, 10, and 11 according to type of steels group and line energies. Although for all three steels the same line energies were applied, only the specimens from Manufacturer1 API X-65 steel were cracked under the majority of test conditions (Table 9).

Table 9. HIC test results for Manuf1 API X-65 / 11,90 mm.

Manuf1 API X-65 / 11,90 mm.		
Parameter	Line Energy (kj / cm)	Test Result
1	5.3	CRACKED
2	6.0	CRACKED
3	7.2	CRACKED
4	8.0	OK
5	9.0	CRACKED
6	10.3	CRACKED
7	10.8	CRACKED
8	12.0	OK
9	13.5	OK

Table 10. HIC test results for Manuf2 API X-65 / 11,91 mm.

Manuf2 API X-65 / 11,91 mm.		
Parameter	Line Energy (kj / cm)	Test Result
10	5.4	OK
11	6.0	OK
12	7.0	OK
13	8.0	OK
14	9.0	OK
15	10.3	OK
16	10.8	OK
17	12.0	OK
18	13.5	OK

Table 11. HIC test results for Manuf2 API X-65 / 14,27 mm.

Manuf2 API X-65 / 14,27 mm.		
Parameter	Line Energy (kj / cm)	Test Result
19	5.3	OK
20	6.0	OK
21	7.2	OK
22	8.0	OK
23	9.0	OK
24	10.8	OK
25	11.1	OK
26	12.0	OK
27	13.1	OK

4.3. Microscopic Examination

Micrographs of parameter '1' at 100X magnification are shown in Figure 17. Other micrographs of the cracked test specimens are given in the Appendix A. A Computer program was used to measure the crack length and total crack length, whereby a calibration block was utilized to calibrate the program as shown in Figure 16. In these measurements, the calibration factor (the ratio of distance measured with program to real distance) was 1000 (Table 12).

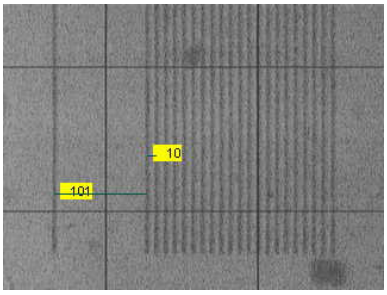

Figure 16. Calibration block photo at 100X magnification

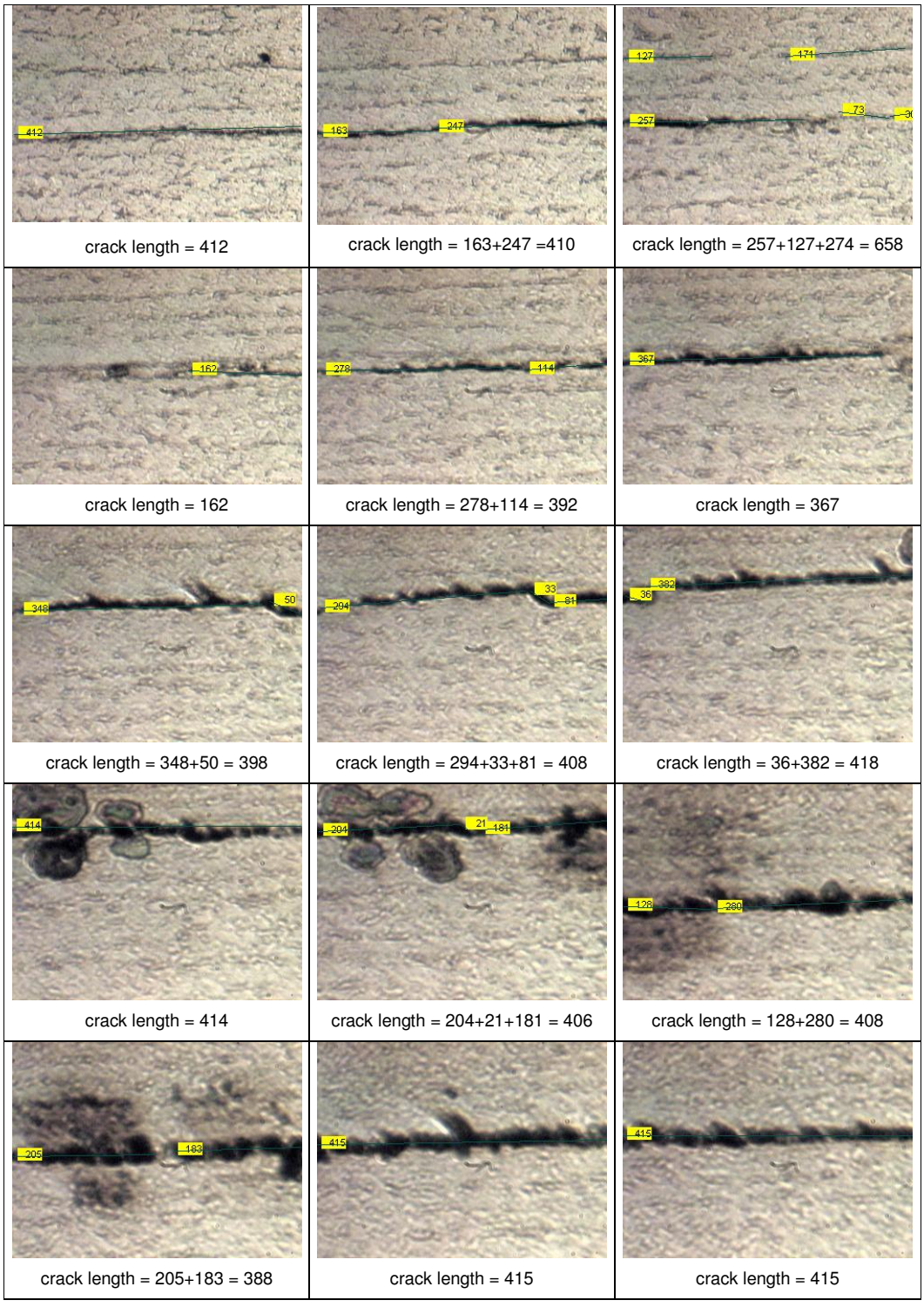

Figure 17. Micrographs of Manuf1 API X-65 steel
for parameter ‘1’ at 100X magnification

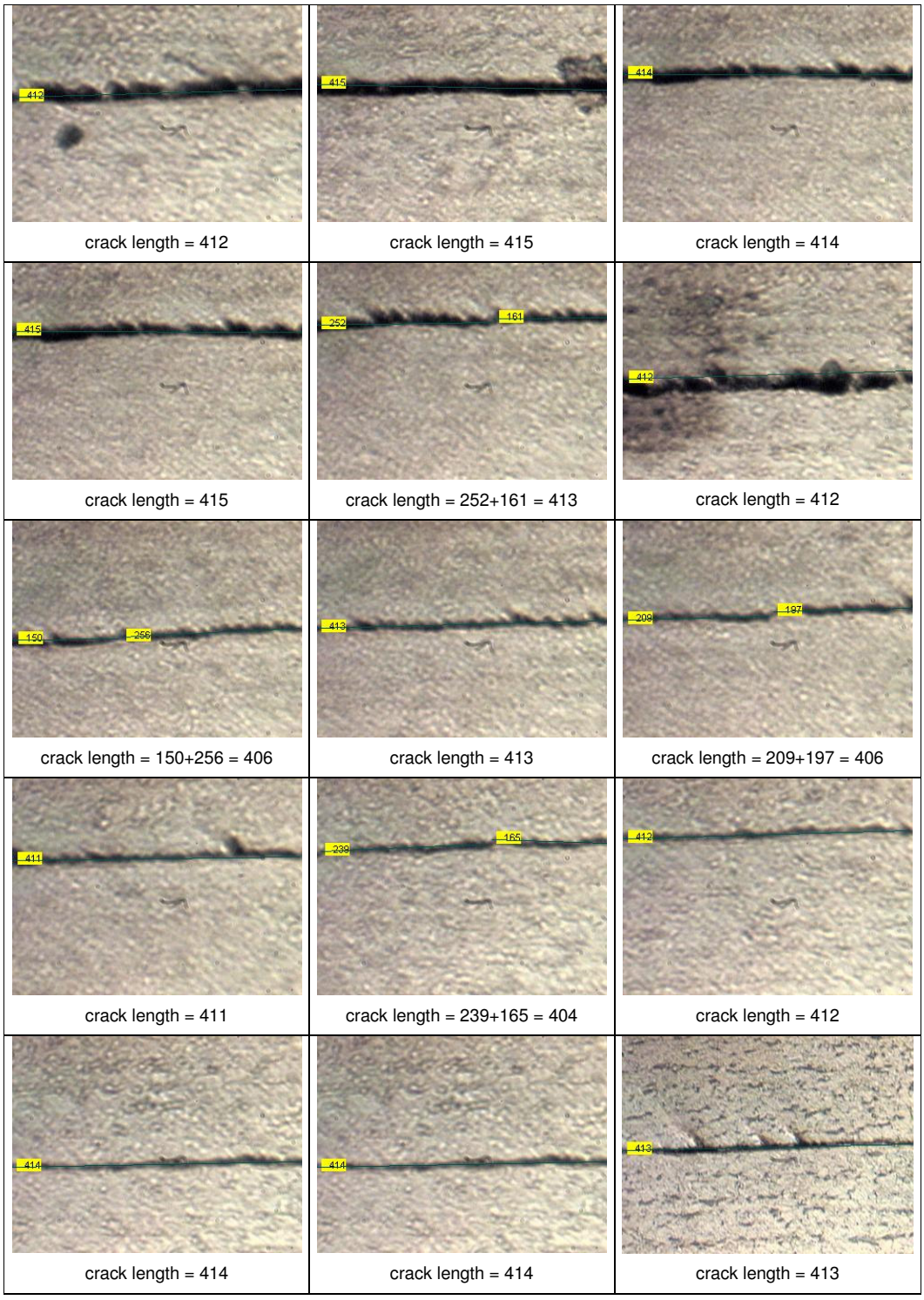

Figure 17 (continued)

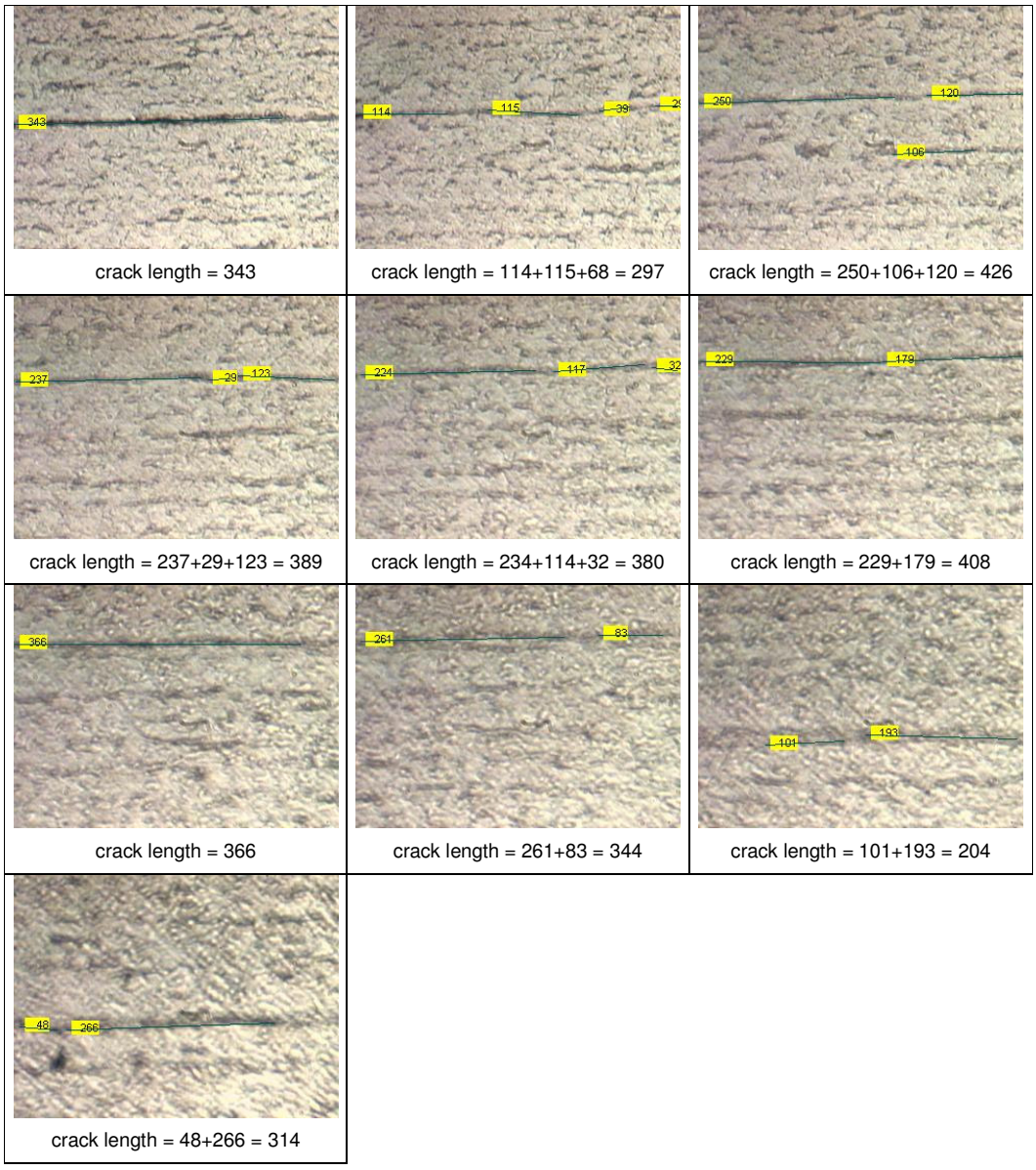

Figure 17 (continued)

Table 12 Total crack lengths of cracked test specimens

Parameter	Crack Length (measured)	Crack Length (mm)	Specimen Length (mm)	CLR (%)
1	15862	15.862	33.33	47.59
2	8370	8.370	33.33	25.11
3	7422	7.422	33.33	22.27
5	14895	14.895	33.33	44.69
6	8035	8.035	33.33	24.11
7	15490	15.490	33.33	46.47

4.4. Hardness Test Results

Hardness test results of specimens are shown in Appendix B. Average hardness values of material, HAZ and weld sections are given in Table 13. In order to determine the hardness effect on the cracking susceptibility, more detailed micro hardness tests according to EN 1043-2 standard (Destructive tests on welds in metallic materials – Hardness test – Part 2: Micro hardness testing on welded joints) were performed and their results are shown in Table 14. Figure 18 illustrates the change of average hardness values for the material, HAZ, and weld regions. From Figure 18, one can conclude that the parameter numbered '1', '5', and '7' yielded the highest hardness.

Table 13. Hardness test results of all parameters

Parameter	M	H	W
1/ HV 10	196	203	267
2 / HV 10	199	212	238
3 / HV 10	199	206	241
4 / HV 10	219	207	234
5 / HV 10	200	207	225
6 / HV 10	202	209	233
7 / HV 10	217	218	248
8 / HV 10	199	205	223
9 / HV 10	202	205	229

Parameter	M	H	W
10 / HV 10	196	200	238
11 / HV 10	195	196	230
12 / HV 10	197	199	225
13 / HV 10	192	182	226
14 / HV 10	200	184	223
15 / HV 10	199	186	217
16 / HV 10	196	195	225
17 / HV 10	200	194	231
18 / HV 10	204	188	220

Parameter	M	H	W
19 / HV 10	193	204	234
20 / HV 10	199	200	219
21 / HV 10	198	194	218
22 / HV 10	200	190	219
23 / HV 10	199	191	215
24 / HV 10	199	195	218
25 / HV 10	200	193	218
26 / HV 10	200	188	217
27 / HV 10	199	193	215

Table 14. Microhardness test results for Manuf1 API X-65 / 11,90 mm.

Parameter	1 HV 0.5	2 HV 0.5	3 HV 0.5	4 HV 0.5	5 HV 0.5	6 HV 0.5	7 HV 0.5	8 HV 0.5	9 HV 0.5
W	258.21	230.15	239.77	202.94	243.98	220.45	212.65	226.16	228.51
H	257.19	215.75	216.99	212.16	231.97	209.15	218.63	211.14	214.95
M	204.23	192.75	196.25	192.35	205.38	203.65	200.19	207.95	205.78

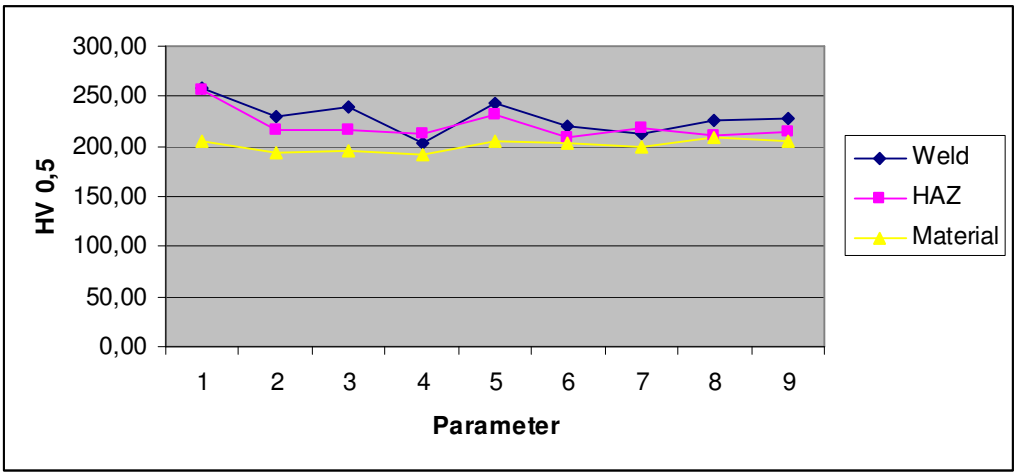

Figure 18. Variation of microhardness as a function of line energy.

4.5. Impact Toughness Test Results

Impact toughness test results are tabulated in Table 15. The values included in this table are average of three measurements and given also in graphical form in Figure 19.

Table 15. Impact toughness test results

Parameter	Average Energy for Welds (J)		
	Manuf1 API X-65 11,90 mm.	Manuf2 API X-65 11,91 mm.	Manuf2 API X-65 14,27 mm.
1 – 10 – 19	194	179	227
2 – 11 – 20	203	218	227
3 – 12 – 21	144	192	151
4 – 13 – 22	86	56	199
5 – 14 – 23	61	188	251
6 – 15 – 24	41	81	237
7 – 16 – 25	58	136	184
8 – 17 – 26	91	144	228
9 – 18 – 27	98	117	148

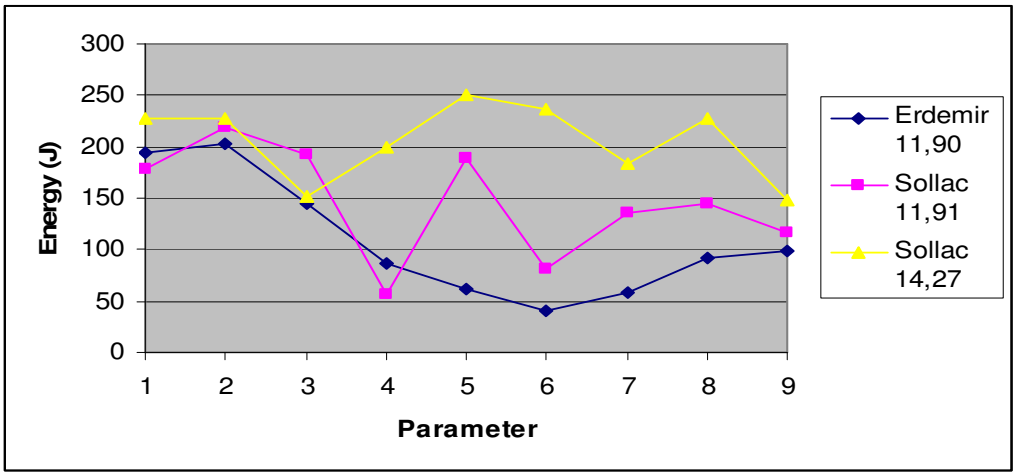

Figure 19. Variation of impact toughness as a function of line energy.

4.6. Chemical Analysis

Chemical analysis of the test specimens for material and weld regions are tabulated in Appendix C. Carbon equivalent values for all specimens were calculated and indicated in Table 16.

Table 16. Carbon equivalent values of all parameters

Parameter	CE	Parameter	CE	Parameter	CE
1	0.386	10	0.231	19	0.233
2	0.371	11	0.233	20	0.233
3	0.371	12	0.234	21	0.233
4	0.377	13	0.251	22	0.234
5	0.416	14	0.224	23	0.231
6	0.400	15	0.217	24	0.235
7	0.416	16	0.232	25	0.235
8	0.391	17	0.233	26	0.233
9	0.399	18	0.236	27	0.233

4.7. SEM Analysis

Cracked test specimen Manufacturer1 steel API X-65 11,90 mm ('1' parameter), was examined under scanning electron microscope at 500X magnification. As seen from Figure 20 cracks are transgranular and their starting points are free from nonmetallic inclusions.

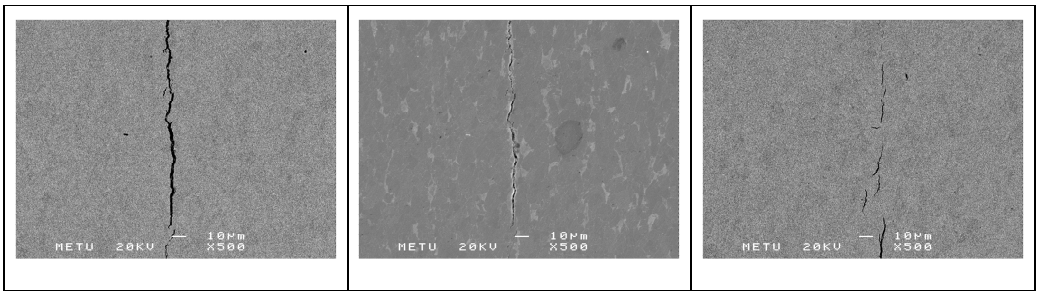

Figure 20. SEM views at 500X magnification

4.8. Grain Size

In order to compare the grain sizes of steels delivered by two different steel producers, the micrographs shown in Figure 21 were taken at 100X magnification under the light microscope. Grain size measurements were done according to ASTM E112 Standard (Standard test methods for determining average grain size) and shown in Figure 21. It is evident that the Manufacturer2 steel which was free from cracking has smaller grain size compared to Manufacturer1 steel.

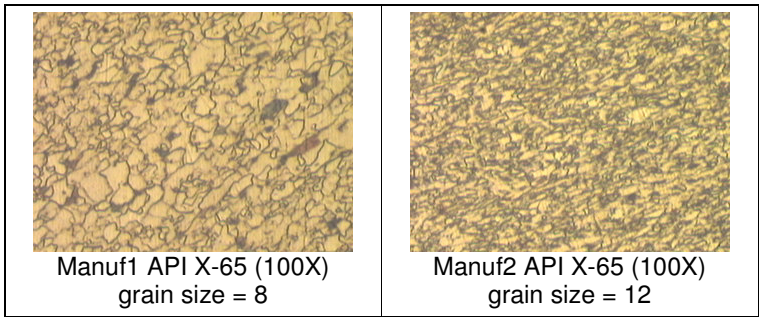

Figure 21. Microstructure of two different steel

5. DISCUSSION

5.1. Cracked Specimen Group Analysis

In order to reveal the possible correlations between the hardness, carbon equivalent of steel, and the crack length, a group analysis was applied through arranging these data in Table 17. In addition, the variation of carbon equivalent together with the hardness of HAZ as a function of line energies is given in Figure 22. The information which can be inferred from the present data can be summarized as follows;

- The specimens with longer crack length have also higher hardness in HAZ and larger carbon equivalents. This is particularly the case for parameters '1', '5', and '7'.
- The variations of crack length and HAZ hardness with line energy included in Figure 23 are also in support of this conclusion.
- However, it appears to be not possible to define threshold values for hardness and carbon equivalent that would be large enough to induce hydrogen cracking.

Table 17. Crack length, hardness and carbon equivalent values as a function of line energies

Parameter	Crack Length (mm)	Material Hardness (HV 0,5)	HAZ Hardness (HV 0,5)	Weld Hardness (HV 0,5)	Carbon Equivalent
1	15.86	46.08	257.19	58.26	0.386
2	8.37	43.49	215.75	51.93	0.371
3	7.42	44.28	216.99	54.10	0.371
4	-	43.40	212.16	45.79	0.377
5	14.89	46.34	231.97	55.05	0.416
6	8.03	45.95	209.15	49.74	0.400
7	15.49	45.17	218.63	47.98	0.416
8	-	46.92	211.14	51.03	0.391
9	-	46.43	214.95	51.56	0.399

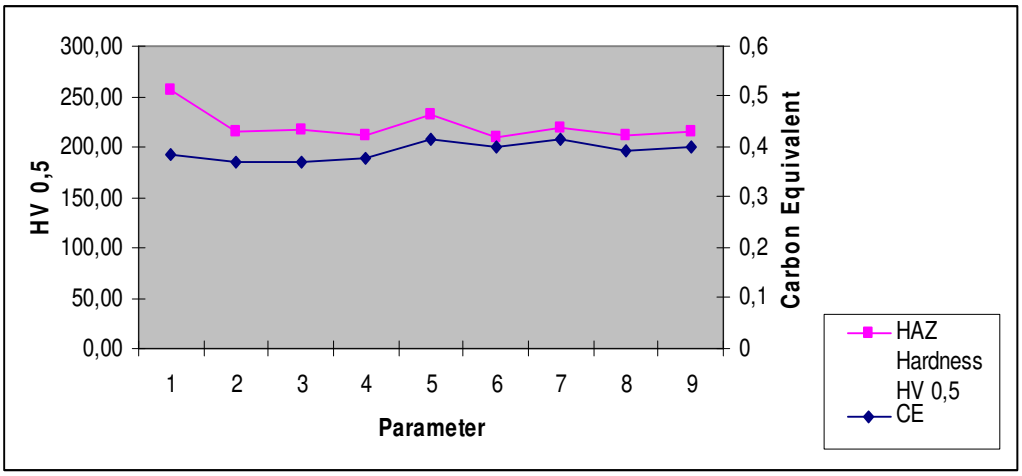

Figure 22. Variation of hardness and carbon equivalent as a function of line energy.

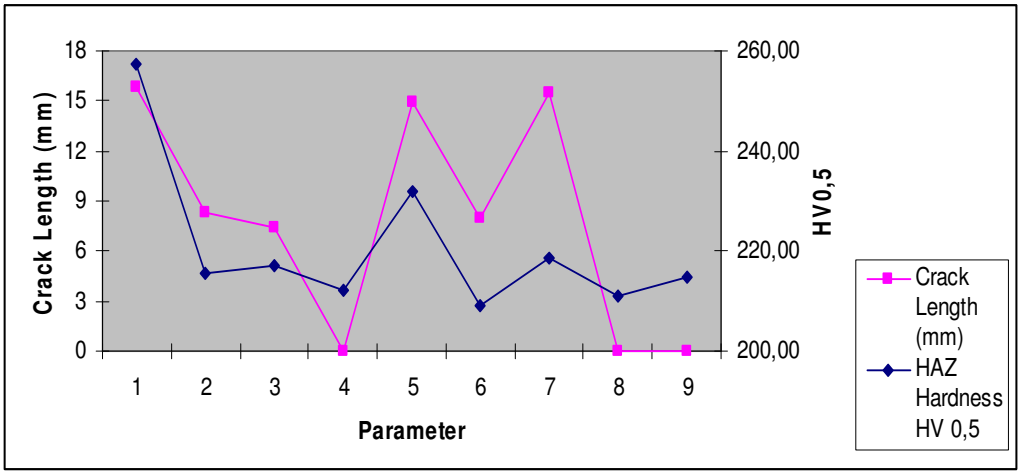

Figure 23. Variation of hardness and crack length as a function of line energy.

5.2. Effect of Metallurgical Variables

Steels delivered by two different steel producers show different cracking behavior under wet H_2S environment. First steel group (Manuf2 API X-65) showed resistance to cracking while the other one (Manuf1 API X-65) welded with some line energies cracked.

The carbon equivalent values calculated from the average chemical compositions of steels are given in Table 18. As seen, the cracked steel has higher carbon equivalent compared with other two. The conclusion which can be drawn at this stage is that a strict control of chemical composition of steel is of primary significance as far as the resistance against the HIC is concerned.

Table 18. Average chemical compositions of steels

Elements	Manuf1 API X-65 11,90 mm.	Manuf2 API X-65 11,91 mm.	Manuf2 API X-65 14,27 mm.
%C	0.094	0.040	0.040
%Si	0.196	0.179	0.190
%Mn	1.557	1.052	1.041
%P	0.015	0.011	0.011
%S	0.008	0.001	0.001
%Ni	0.031	0.173	0.219
%Cr	0.025	0.020	0.020
%Mo	0.115	0.000	0.000
%Cu	0.036	0.017	0.014
%Al	0.044	0.033	0.034
%Nb	0.052	0.060	0.059
CE	**0.392**	**0.232**	**0.233**

Evidently, the grain size of steel is another important factor which can directly be correlated with susceptibility to cracking. As indicated in Figure 21, the Manufacturer2 API X-65 steel which resisted the cracking under all conditions tested has finer grains compared to Manufacturer1 API X-65.

5.3. Effect of Hardness

Variation of average hardness values of steels for three regions (material, HAZ and weld) are depicted in Figures 24, 25, and 26. For all parameters the hardness values of Manufacturer1 steel are higher than that of the other two. At this stage of discussion it would be worthwhile to compare data included in Table 9 and Figures 24 to 26. Even though there is not a one-to-one correlation exist, it can generally be claimed that the susceptibility to HIC increases with increasing hardness.

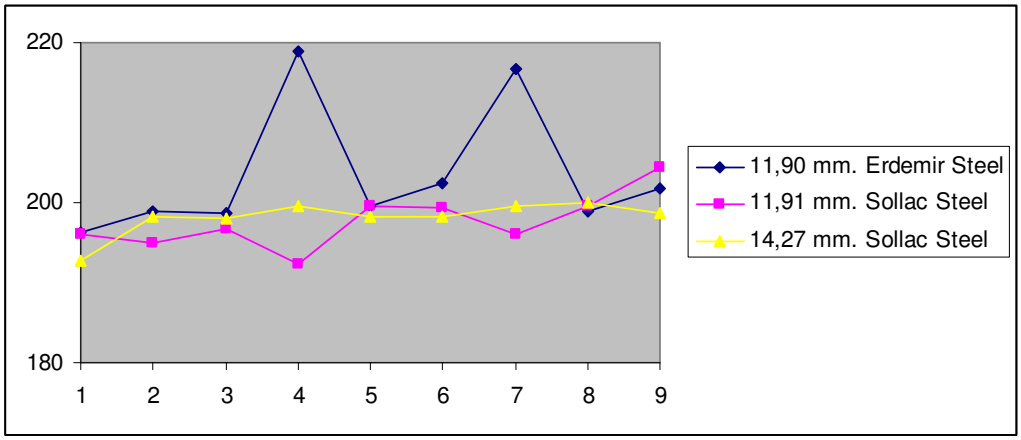

Figure 24. Variation of material hardness values as a function of line energy

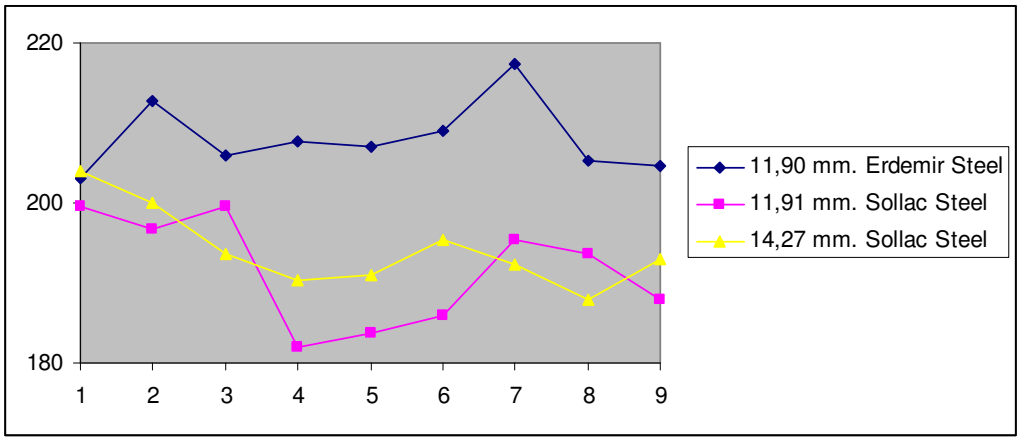

Figure 25. Variation of HAZ hardness values as a function of line energy

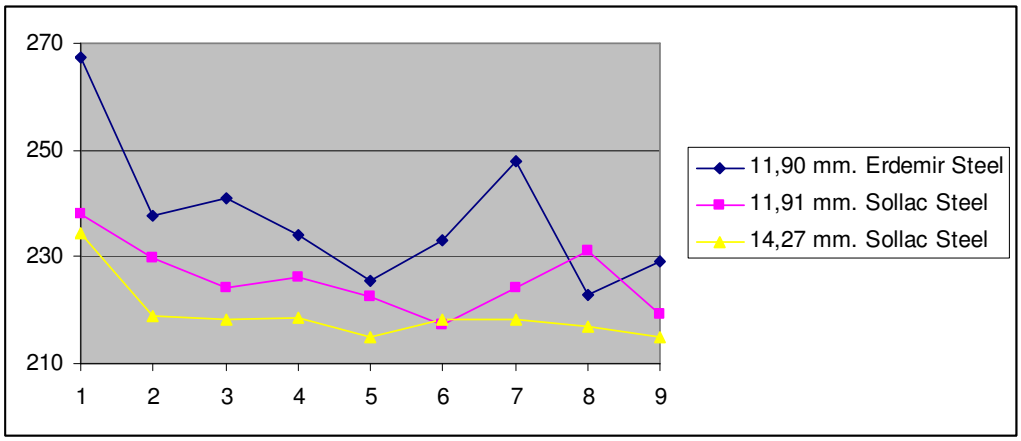

Figure 26. Variation of weld hardness values as a function of line energy

5.4. Effect of Welding Parameters

There is no direct relation between welding parameters and HIC susceptibility of steel as indicated by comparison of the line energy values with crack lengths in Table 19. However, the welding parameters that increase the hardness of the HAZ may induce susceptibility to HIC. Beside the carbon equivalents, the cooling rate of HAZ after welding has to be taken into consideration as an additional factor which would control the hardness.

The relationship between the carbon equivalent and hardness value is determined and shown in the Figure 22. Carbon equivalent of welding wire is the only parameter which affects the chemical composition of the weld and HAZ. The high value of carbon equivalent of welding wire can induce HIC.

Cooling rates of HAZ after welding is an additional factor which controls the increase in hardness. On the other hand, the cooling rate depends on the line energy, thickness and the temperature of welded plates. In order to prevent fast cooling, preheating of parts to be welded would be recommended. In addition, the higher line energies may also cause reduction in cooling rate. Like the thick section parts, larger welding area may also be useful to have slow cooling. The welding area can be enlarged by reducing the welding speed and increasing the current.

Table 19. Relation of welding parameters and crack length

Parameter	Crack Length (mm)	Weld Speed (cm/min)	Voltage (V)	Current (A)	Line Energy (kj/cm)
1	15.86	270	800	30	4.77
2	8.37	240	800	30	5.40
3	7.42	200	800	30	6.48
4	-	90	400	30	7.20
5	14.89	80	400	30	8.10
6	8.03	70	400	30	9.27
7	15.49	50	300	30	9.72
8	-	45	300	30	10.80
9	-	40	300	30	12.15

6. CONCLUSIONS

This study has led to the following conclusions;

1. Metallurgical parameters are more effective than welding parameters in determining HIC susceptibility of steel in wet H_2S environments.

2. Carbon equivalent and average grain size values are the predominant metallurgical parameters that affect the HIC resistance. Fine grained steels with low carbon equivalent are more resistant against cracking in wet H_2S environments.

3. There is a direct relation between carbon equivalent and HAZ hardness values. However, there is not a threshold hardness value below which the cracking could be eliminated.

4. After welding, slow cooling rates may produce softer microstructures. Therefore, the welding parameters that cause slow cooling rates may be preferred to prevent HIC.

REFERENCES

1) N.A. Fayad, “The Corrosion Behavior of Low - Alloy Steels in Oil Well Fluids” Master Thesis in Metallurgical Engineering, METU, Ankara / Turkey

2) H.Y. Liou, R.I. Shieh, F.I Wei and S.C. Wang “Roles of Microalloying Elements in HIC Resistant Property of High Strength Low Alley Steels”, Corrosion- Vol. 49, No.5, May 1993, p.389 - 398

3) M. Elboujdarni, V.S. Sastri, and R.W. Revie “Field Measurement of Hydrogen in Sour Gas Pipelines”, corrosion Vol. 50, No.8, August 1994, p.636 - 640

4) A. Ikeda, T. Kaneke, L. Hashimoto, M. Takeyama, Y. Sumitomo, “Development of HIC Resistant Steels and HIC Test Methods for Hydrogen Sulfide Service” T. Proc Symp. Effect of Hydrogen Sulfide on Steel, 22.nd Ann. Cof Metallurgists, Canadian Institute of Mining and Metallurgy, Edmonton, Alta, Canada, 1983.

5) NACE Standard TN-02-84, “Test Method Evaluation of Pipeline Steels for Resistance to Stepwise Cracking” (Houston, TX, Nace, 1984)

6) L. Albarran, A. Aguilar, L. Martinez and H.F. Lopez “Corrosion and Cracking Behavior in an API X-80 Steel Exposed to Sour Gas Environments”, Corrosion Vol.58, No.9, September 2002, p.783 - 792

7) Denny A. Jones, “Principles and Prevention of Corrosion” Prentice Hall, Upper Saddle River, NJ 07458, Second Edition, 1996, p.337 -340

8) R.D McCright “Effects of Environmental Species and Metallurgical Structure on the Hydrogen Entry into Steel” pp 306-325 the Ohio State University Corrosion Center, Columbus, Ohio

9) M. Smialowski, “Hydrogen Blistering and Sulfide Microcracks” p.405 - 422 Warsaw, Poland

10) R.A Oriani, “A Decohesion Theory for Hydrogen Induced Crack Propagation” US Steel Research Laboratory Monroeville, Pennsylvania, p.351 - 358

11) T. Hara, H. Asahi and H. Ogawa, “Conditions of Hydrogen Induced Corrosion Occurrence” of X-65 Grade Line Pipe Steels in Sour Environment”, Corrosion Vol.60, No 12, December 2004, p.1113 - 1121

12) M. Kimura, N. Totsuka, T. Kursu, I. Hane, Y. Nakai “Effect of Environmental Factors on Hydrogen Permeation in Line Pipe Steel” Corrosion 85, paper number 237, March 1985, p.529 - 541

13) G.J. Biefer “The Stepwise Cracking of Line Pipe Steels in Sour Environments” Materials Performance, Vol.21, No.6, June 1982, p.19 - 34

14) E.M. Moore, J.J. Warga, “Materials Performance” Vol.15, No.6 pp 17 (1976)

15) E. Miyoshi, T. Tanaka, F. Terasaki, A. Ikada, “Hydrogen Induced Cracking of Steels under Wet Hydrogen Sulfide Environment” Transactions of the ASME: Journal of Engineering for Industry, Vol.898, p.1221, (1976)

16) T. Taira, Y. Kobayeshi, H. Inagaki, T. Watanabe, “Sulfide Corrosion of Line Pipe for Sour Gas Service” NACE National Conference, 1979, Atlanta, Unpublished paper, No: 171

17) T.P. Greenveld, R.R. Fissler, “Hydrogen Induced Damage in Sour Gas Gathering Lines” Proc. Nace Western Regron Conf. 1979, Calgay

18) T. Nishimvra, H. Inagaki, M. Tanimura, “Hydrogen Cracking in Sour Gas Pipe Line Steels” Paper no. 3E9 Second Intl. Cong on Hydrogen in Metals, 1977, Paris

19) B.E. Wilde, C.D. Kim, E.H. Pleps, “Some Observations on the role of Inclusions in the Hydrogen Induced Blister Cracking of Line Proc. Steels in Sulfide Environments” NACE National Conference, 1980, Chicago

20) T. Tara, Y. Kobayeshi, “Study of HIC Testing Method”, Technical note for T-1 F-20, SWC Task Group, 1980

21) A. Ikeda, Y. Morita, F. Terasaki, M. Takeyama, “On the Hydrogen Induced Cracking of Line Pipe Steel under Wet Hydrogen Sulfide Environment” Paper no: 4A7 Second Int.Cong on Hydrogen in Metals, 1977, Paris

22) M. Iino, “The Extension of Hydrogen Blister Crack Array in Line Pipe Steels”, Metallurgical Transactions, Vol.9A, No.11, 1978, p.1581

23) A. Ikeda, F. Terasaki, M. Takeyama, I. Takeuchi, Y. Mara, “Hydrogen Induced Creaking Susceptibility of Various Steel Line Pipe in the Wet, H_2S

Environment", NACE National Conference, 1978, Houston, Unpublished paper, No: 43

24) A. Sandberg, W. Lobertg, "Thermomechanical Process of Microalloyed Austenite", Metallurgical Society of AIME, p.405, 1982, Pittsburg

25) R.K. Amine, F.B. Prekering, "Thermomechanical Process of Microalloyed Austenite", Metallurgical Society of AIME, p.377, 1982, Pittsburg

26) B. Butto, C.M. Sellars, "Materials Science and Technology, 2", 1986, p.146

27) R.S. Parmer, "Welding Processes and Technology", Khanna Publishers, New Delhi, 1992

28) P.T. Hould croft, Submerged Arc Welding, second ed., Abington Publishing, Cambridge, England, 1989

29) Submerged Arc Welding, last date accessed: 08.10.2006, http://www.twi.co.uk/j32k/protected/band_3/jk5.html

30) George Linnert, "Welding Metallurgy" GML Publications, South Carolina, USA, Fourth Edition, 1994, p.505 - 511, 653 - 698

APPENDIX A: MICROGRAPHS OF CRACKED SPECIMENS

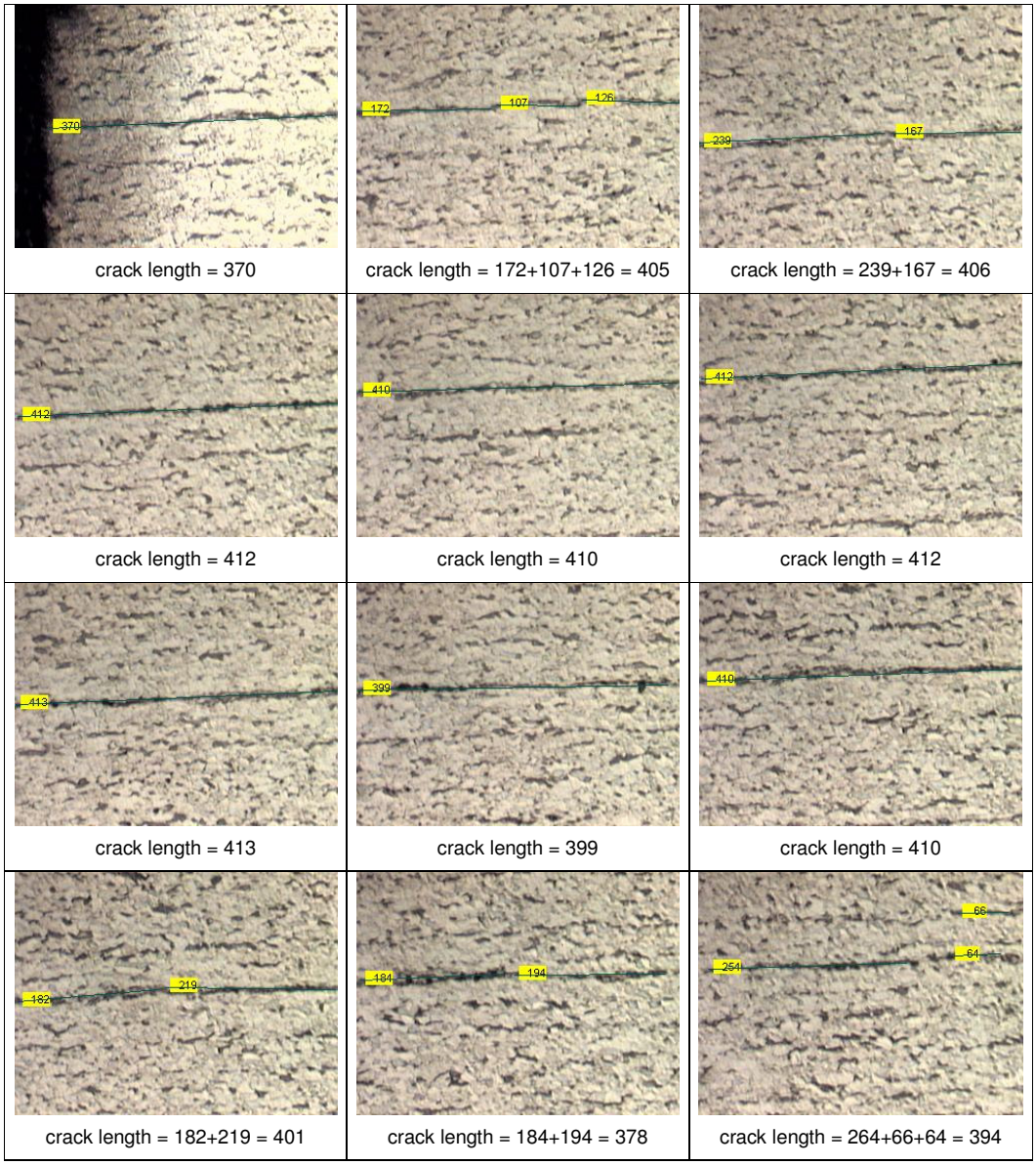

Figure 1 Micrographs of Manuf1 API X-65 steel
for parameter 2 at 100X magnification

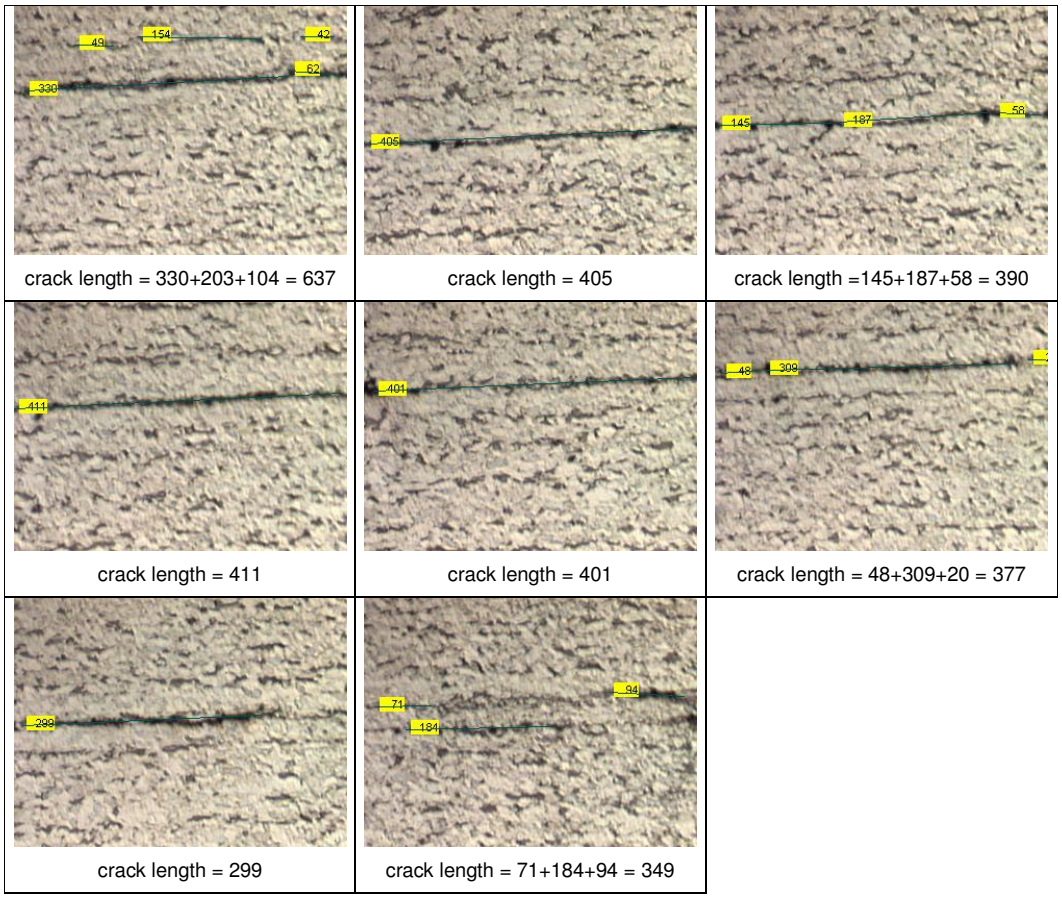

Figure 1 (continued)

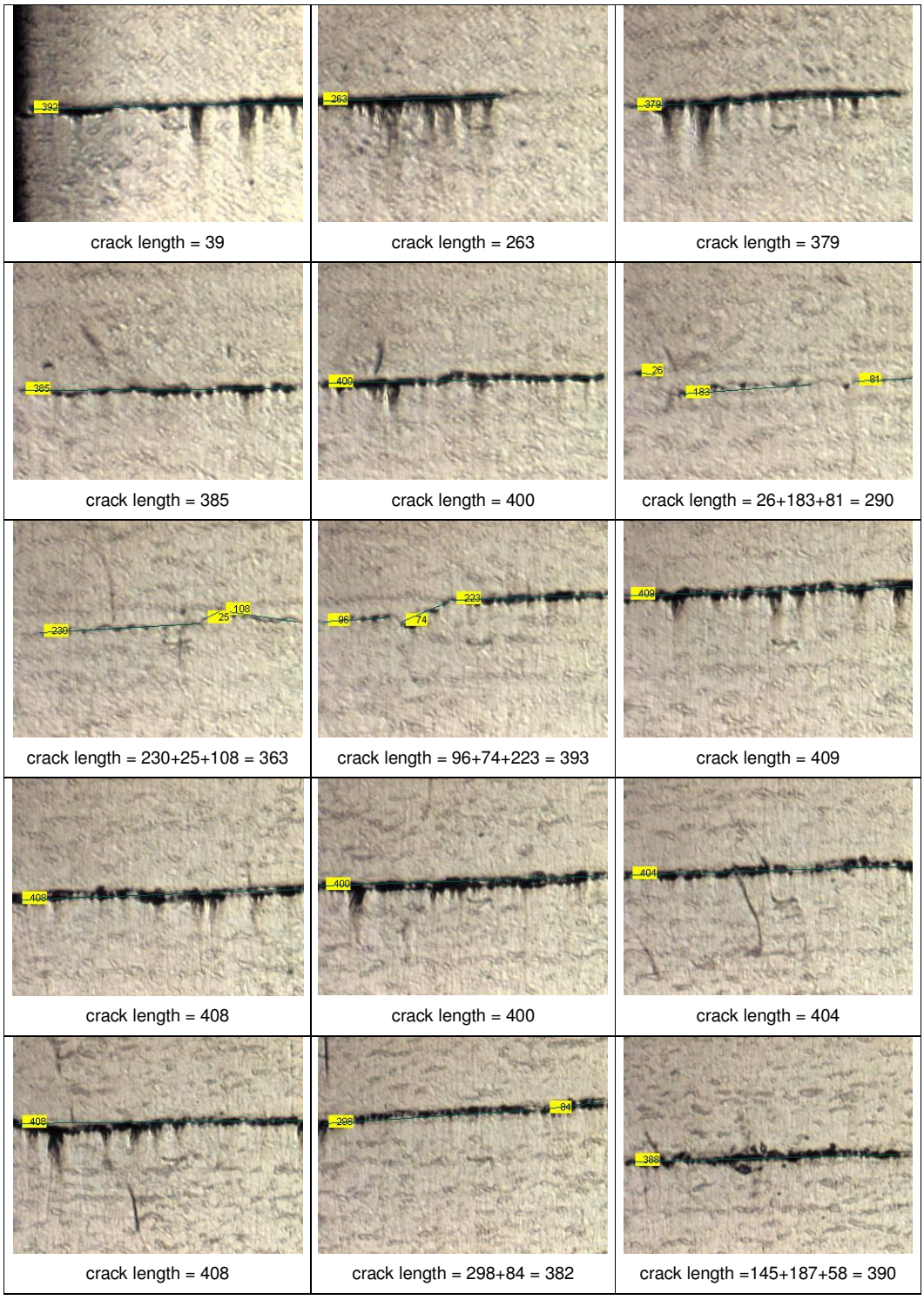

Figure 2 Micrographs of Manuf1 API X-65 steel
for parameter 3 at 100X magnification

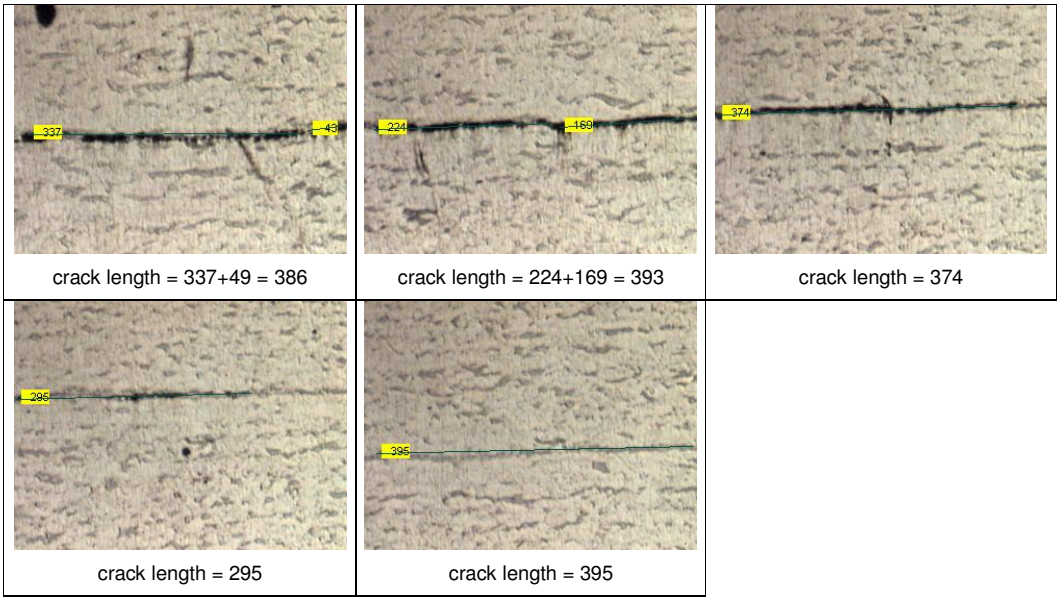

crack length = 337+49 = 386 | crack length = 224+169 = 393 | crack length = 374

crack length = 295 | crack length = 395

Figure 2 (continued)

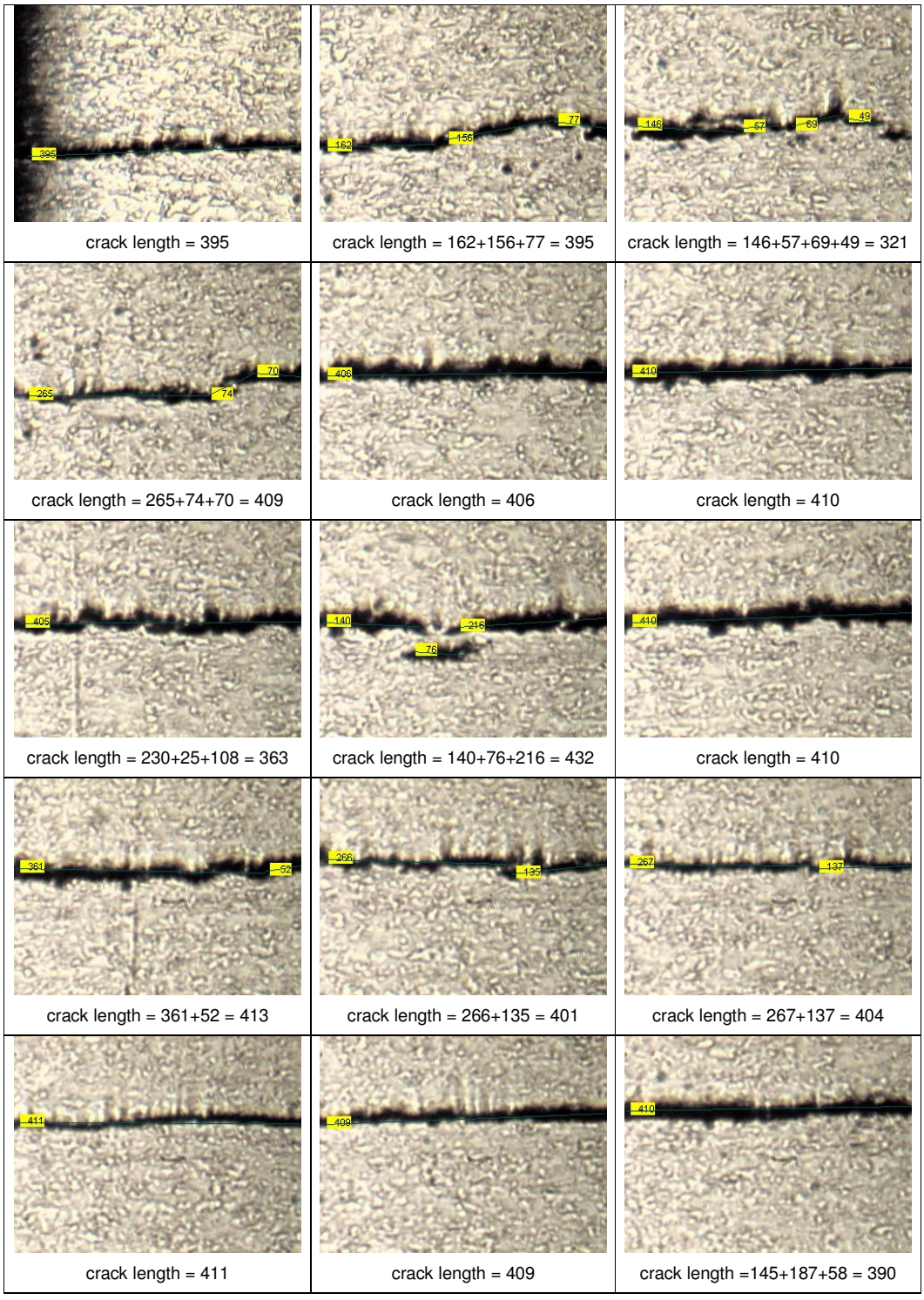

Figure 3 Micrographs of Manuf1 API X-65 steel
for parameter 5 at 100X magnification

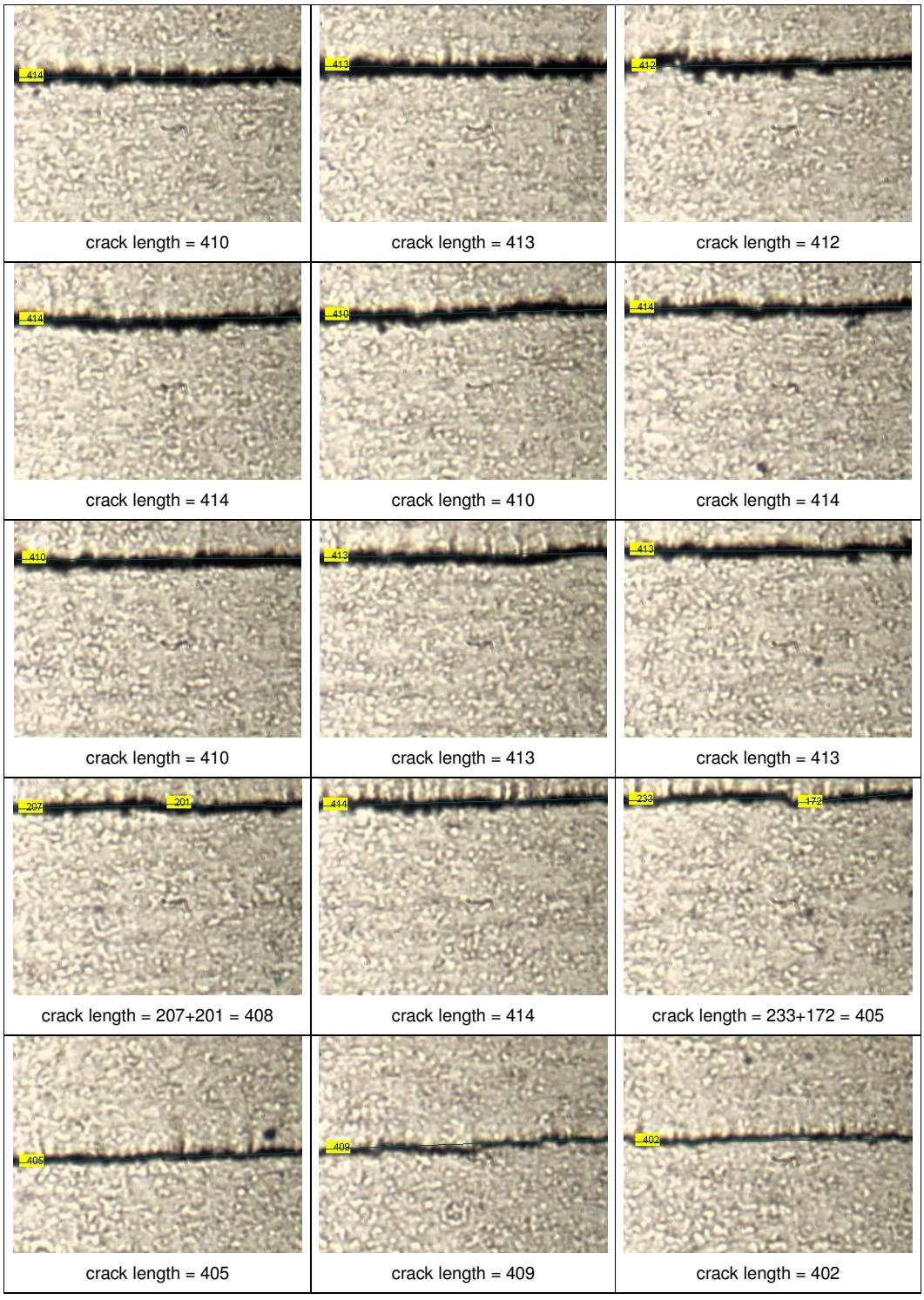

Figure 3 (continued)

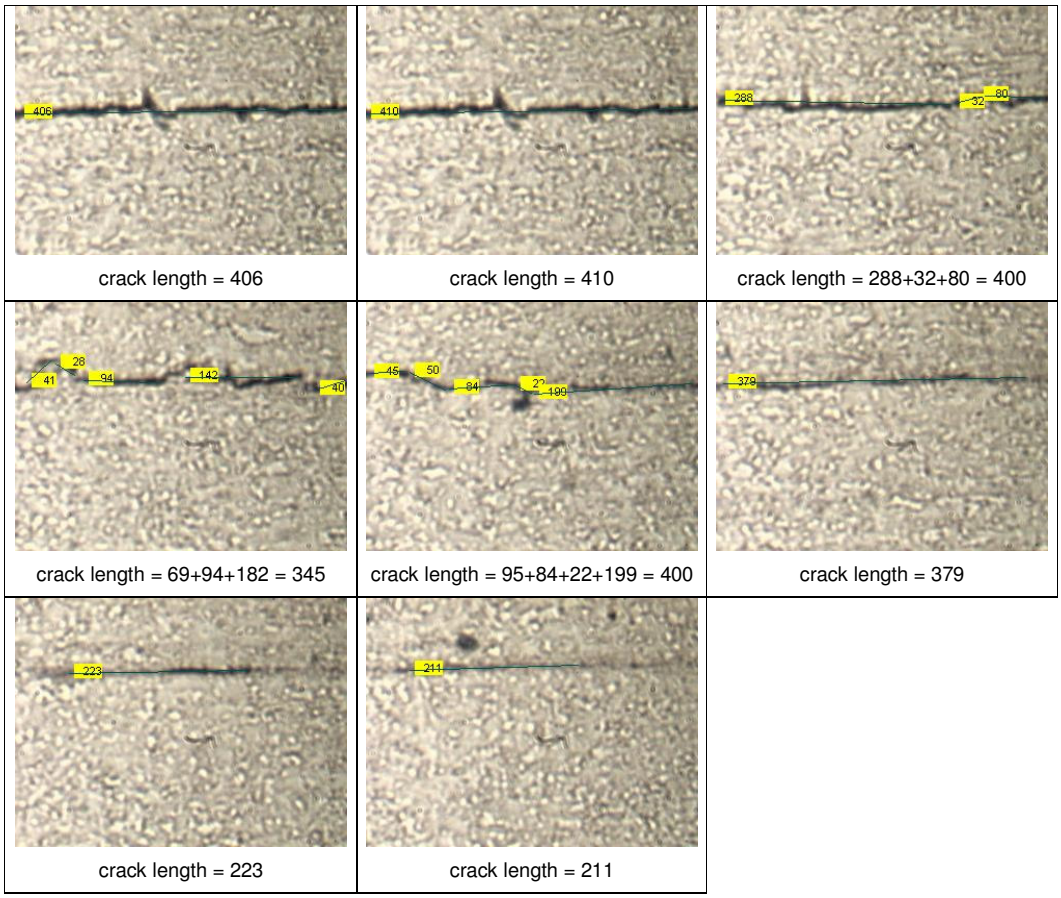

Figure 3 (continued)

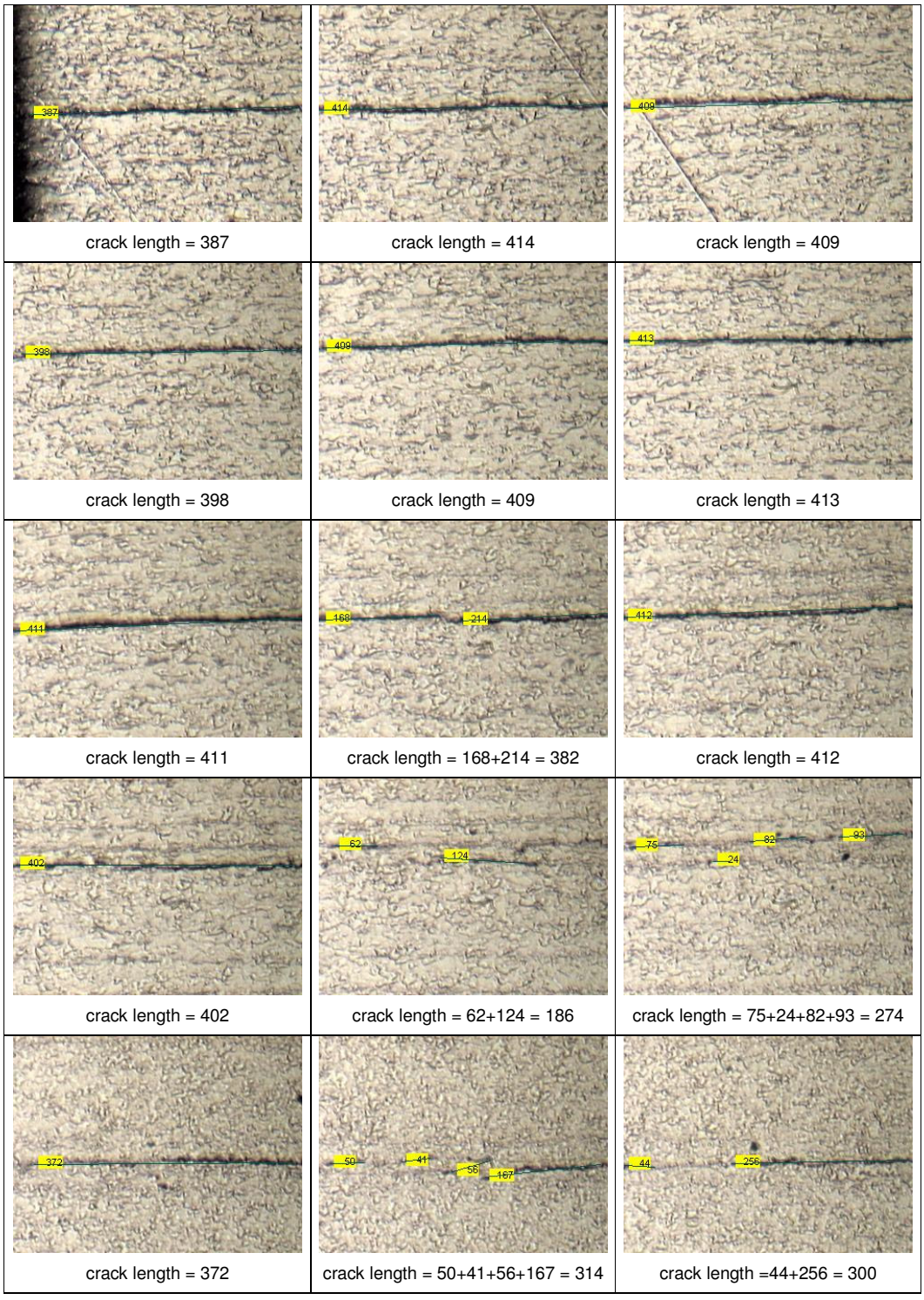

Figure 4 Micrographs of Manuf1 API X-65 steel
for parameter 6 at 100X magnification

crack length = 405

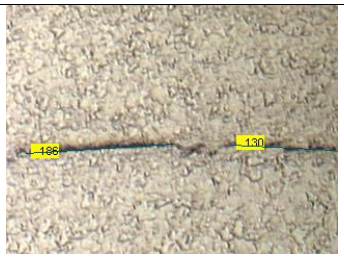

crack length = 186+130 = 316

crack length = 405

crack length = 405

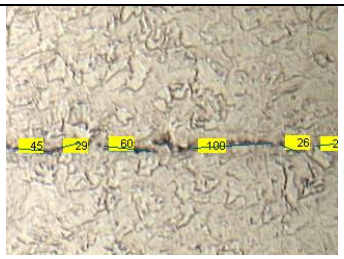

crack length = 45+29+60+146 = 280

Figure 4 (continued)

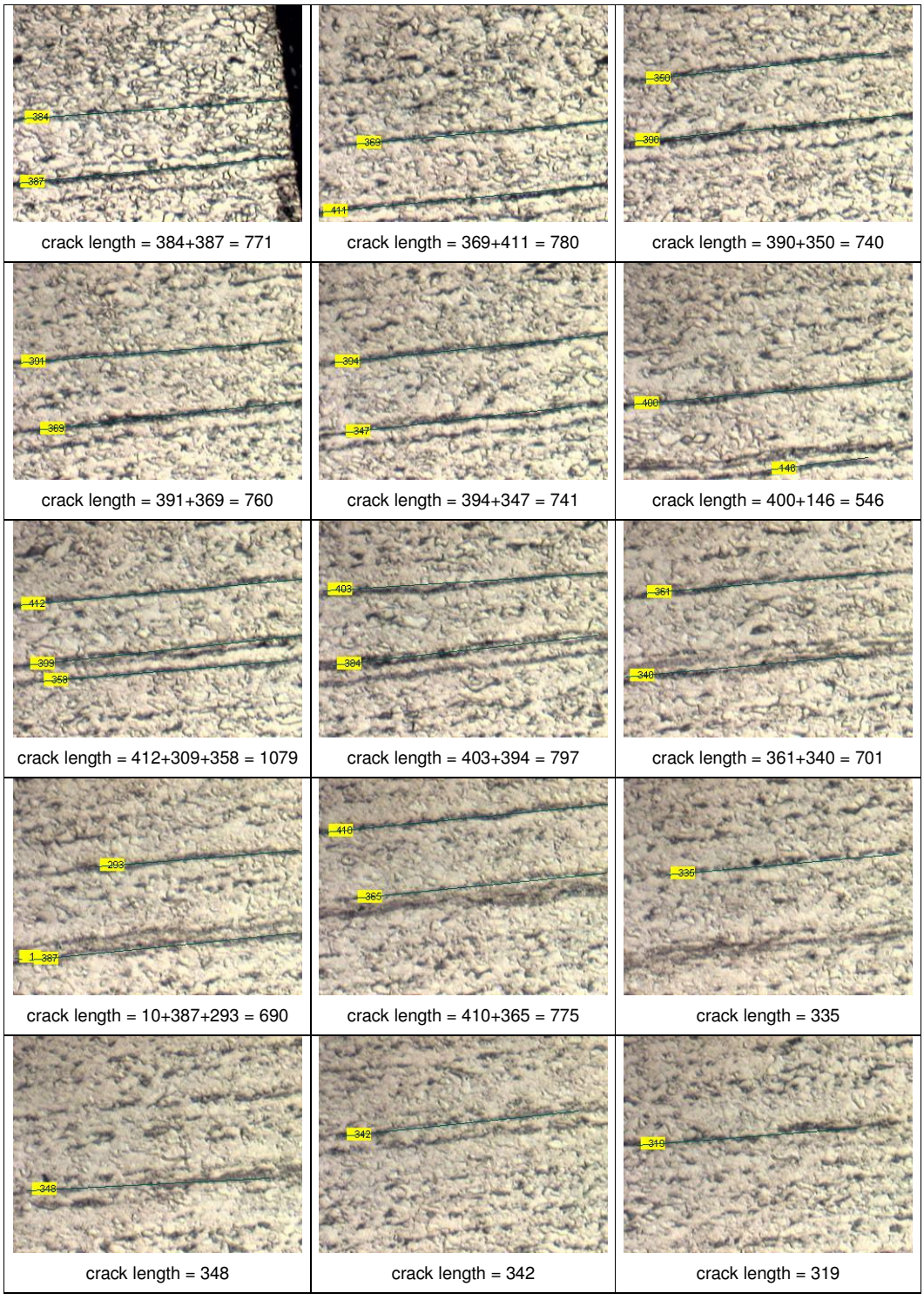

Figure 5 Micrographs of Manuf1 API X-65 steel
for parameter 7 at 100X magnification

crack length = 390

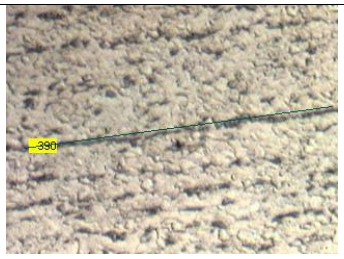

crack length = 390

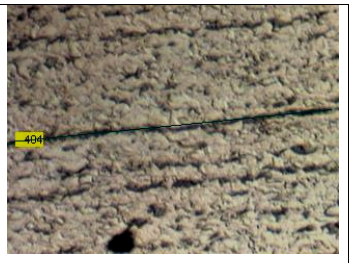

crack length = 404

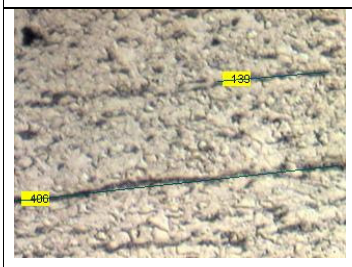

crack length = 406+139 = 545

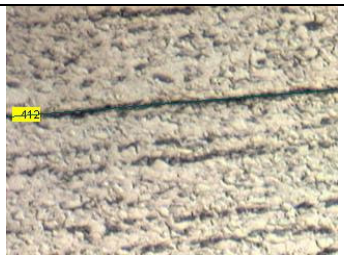

crack length = 412

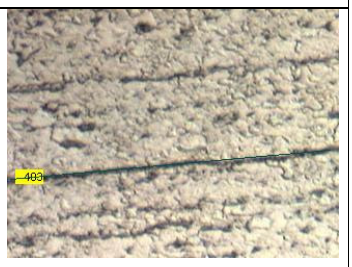

crack length = 403

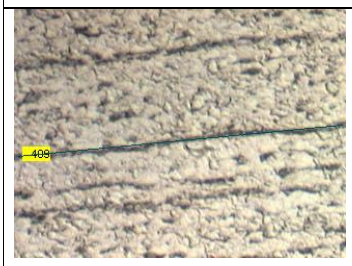

crack length = 409

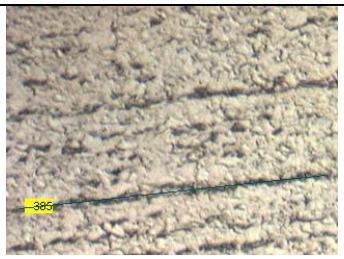

crack length = 385

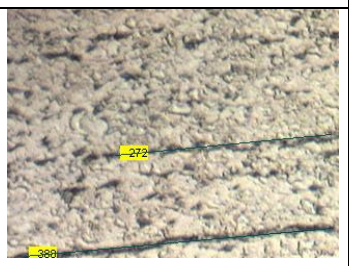

crack length = 388+272 = 660

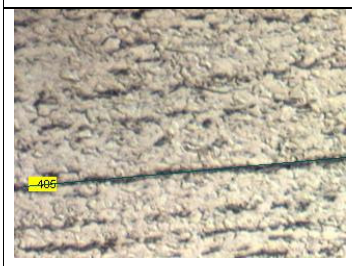

crack length = 405

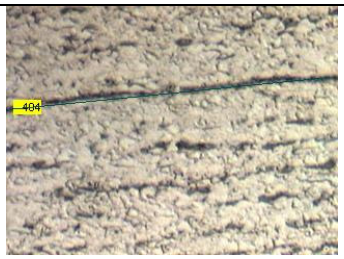

crack length = 404

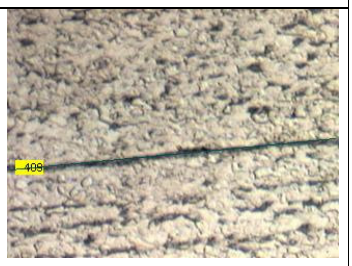

crack length = 409

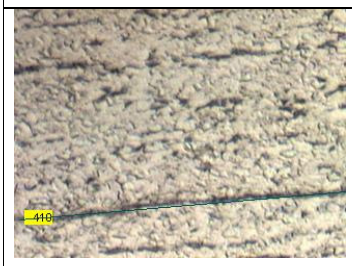

crack length = 410

Figure 5 (continued)

APPENDIX B: HARDNESS VALUES OF TEST SPECIMENS

Table 1 HV 10 Hardness Values of All Specimens

Test Area	Material			HAZ			Weld			Average	Average	Average
Location No	1	2	3	4	5	6	7	8	9	Material	HAZ	Weld
parameter 1 HV 10	199	194	196	203	191	215	255	275	272	196	203	267
parameter 2 HV 10	202	199	196	211	213	214	238	236	239	199	212	238
parameter 3 HV 10	204	195	197	205	201	212	241	237	245	199	206	241
parameter 4 HV 10	221	219	217	206	210	207	233	234	235	219	207	234
parameter 5 HV 10	203	197	199	207	211	203	223	226	227	200	207	225
parameter 6 HV 10	205	202	200	207	211	209	233	230	236	202	209	233
parameter 7 HV 10	208	219	223	220	215	217	243	249	252	217	218	248
parameter 8 HV 10	198	198	201	203	206	207	220	228	221	199	205	223
parameter 9 HV 10	201	200	204	207	197	210	233	229	225	202	205	229
parameter 10 HV 10	193	196	199	196	200	203	236	238	240	196	200	238
parameter 11 HV 10	188	196	201	195	192	203	230	228	231	195	196	230
parameter 12 HV 10	195	194	201	217	189	193	225	220	228	197	199	225
parameter 13 HV 10	193	188	196	191	176	179	225	223	230	192	182	226
parameter 14 HV 10	195	200	204	187	178	186	222	221	225	200	184	223
parameter 15 HV 10	196	199	203	190	183	185	219	216	217	199	186	217
parameter 16 HV 10	195	190	203	207	177	202	217	224	232	196	195	225
parameter 17 HV 10	200	195	204	200	194	187	222	233	238	200	194	231
parameter 18 HV 10	205	205	203	190	189	185	214	221	223	204	188	220
parameter 19 HV 10	194	193	191	202	206	204	234	237	232	193	204	234
parameter 20 HV 10	200	196	199	193	204	203	217	219	221	199	200	219
parameter 21 HV 10	201	194	199	196	191	194	215	217	223	198	194	218
parameter 22 HV 10	201	198	200	189	186	196	217	218	221	200	190	219
parameter 23 HV 10	199	200	196	190	185	198	214	214	217	199	191	215
parameter 24 HV 10	196	195	204	191	196	199	214	220	221	199	195	218
parameter 25 HV 10	199	196	204	193	187	197	214	215	226	200	193	218
parameter 26 HV 10	193	203	204	188	186	190	217	211	223	200	188	217
parameter 27 HV 10	199	196	201	189	192	198	211	215	219	199	193	215

Table 2 HV 0,5 Hardness Values of Cracked Specimens

Location No	Test Area	parameter 1 HV 0,5	parameter 2 HV 0,5	parameter 3 HV 0,5	parameter 4 HV 0,5	parameter 5 HV 0,5	parameter 6 HV 0,5	parameter 7 HV 0,5	parameter 8 HV 0,5	parameter 9 HV 0,5
1	Weld	285.51	232.33	245.84	209.46	221.78	222.26	246.64	229.13	234.90
2		256.17	234.90	250.94	200.24	242.03	217.57	218.01	229.13	217.57
3		263.04	225.32	228.43	207.28	242.03	215.71	177.46	222.89	225.99
4		236.31	225.32	232.33	192.17	253.16	221.60	227.76	225.99	220.98
5		254.62	224.66	239.64	207.28	244.03	230.77	195.19	235.61	225.32
6		263.04	239.64	253.82	192.17	240.92	222.26	181.84	222.26	225.32
7		263.84	232.99	235.61	209.46	256.57	215.71	228.43	218.63	237.02
8		253.82	225.32	232.33	218.63	241.46	215.71	202.90	229.13	237.02
9		247.35	230.95	238.93	189.78	253.78	222.26	235.61	222.89	232.33
10	HAZ	243.10	216.33	212.25	219.25	223.95	211.63	224.66	215.08	218.63
11		243.10	218.63	218.01	232.99	258.03	200.24	227.10	210.03	219.92
12		250.94	210.03	221.60	188.40	228.07	208.84	215.08	211.63	208.84
13		276.02	218.63	218.01	212.25	224.44	212.82	207.68	209.46	211.63
14		272.75	215.08	215.08	207.86	225.32	212.25	218.63	209.46	215.71
15	Material	210.03	202.90	203.43	198.78	213.45	204.98	192.17	198.24	210.03
16		202.90	201.35	197.14	201.35	216.64	205.16	185.92	203.43	203.43
17		192.70	189.78	197.14	197.71	217.08	203.43	194.21	213.45	208.84
18		215.08	185.08	194.12	203.43	218.67	195.19	194.65	216.33	196.60
19		192.70	184.59	188.76	181.84	221.29	206.71	201.83	211.63	202.90
20		192.17	200.24	201.74	184.11	179.63	195.19	209.46	210.03	206.71
21		202.90	185.08	204.98	190.27	179.63	206.71	204.00	214.46	213.45
22		209.46	195.19	197.71	194.65	208.66	205.56	211.63	207.64	213.45
23		216.33	179.63	192.70	178.70	217.08	210.03	211.05	206.13	203.43
24		207.86	203.43	184.59	192.70	181.84	203.43	197.14	198.24	198.78
Average Weld		258.21	230.15	239.77	202.94	243.98	220.45	212.65	226.16	228.51
Average HAZ		257.19	215.75	216.99	212.16	231.97	209.15	218.63	211.14	214.95
Average Material		204.23	192.75	196.25	192.35	205.38	203.65	200.19	207.95	205.78

APPENDIX C: CHEMICAL ANALYSIS OF TEST SPECIMENS

Parameter		%C	%Si	%Mn	%P	%S	%Ni	%Cr	%Mo	%Cu	%Al	%Nb	CE
1	W	0.098	0.468	1.520	0.019	0.006	0.066	0.083	0.103	0.005	0.043	0.045	**0.398**
	M	0.092	0.170	1.562	0.011	0.006	0.031	0.020	0.102	0.033	0.039	0.055	**0.386**
2	W	0.061	0.418	1.491	0.019	0.007	0.057	0.071	0.104	0.030	0.022	0.029	**0.356**
	M	0.090	0.204	1.461	0.015	0.009	0.024	0.026	0.112	0.034	0.048	0.050	**0.371**
3	W	0.080	0.449	1.500	0.019	0.006	0.060	0.078	0.104	0.028	0.026	0.031	**0.378**
	M	0.090	0.204	1.461	0.015	0.009	0.024	0.026	0.112	0.034	0.048	0.050	**0.371**
4	W	0.052	0.473	1.561	0.021	0.006	0.054	0.069	0.106	0.037	0.013	0.027	**0.359**
	M	0.093	0.225	1.478	0.015	0.007	0.023	0.032	0.109	0.027	0.047	0.052	**0.377**
5	W	0.039	0.440	1.544	0.020	0.006	0.048	0.060	0.108	0.036	0.014	0.031	**0.341**
	M	0.110	0.216	1.576	0.014	0.006	0.033	0.027	0.131	0.033	0.044	0.059	**0.416**
6	W	0.052	0.456	1.563	0.021	0.006	0.055	0.072	0.111	0.040	0.012	0.028	**0.361**
	M	0.089	0.143	1.648	0.017	0.008	0.026	0.018	0.110	0.048	0.048	0.040	**0.400**
7	W	0.053	0.479	1.614	0.021	0.007	0.053	0.067	0.118	0.038	0.010	0.028	**0.371**
	M	0.105	0.220	1.614	0.014	0.007	0.033	0.020	0.132	0.033	0.043	0.060	**0.416**
8	W	0.046	0.464	1.542	0.020	0.006	0.054	0.072	0.128	0.052	0.013	0.027	**0.357**
	M	0.089	0.177	1.603	0.018	0.009	0.034	0.025	0.101	0.034	0.035	0.051	**0.391**
9	W	0.082	0.435	1.498	0.021	0.007	0.005	0.070	0.145	0.046	0.002	0.021	**0.386**
	M	0.086	0.201	1.607	0.012	0.007	0.047	0.035	0.124	0.051	0.046	0.054	**0.399**
10	W	0.090	0.410	1.300	0.010	0.000	0.170	0.060	0.120	0.120	0.010	0.020	**0.369**
	M	0.040	0.190	1.030	0.009	0.000	0.210	0.020	0.000	0.020	0.030	0.060	**0.231**
11	W	0.080	0.380	1.270	0.010	0.000	0.170	0.060	0.120	0.130	0.010	0.030	**0.355**
	M	0.040	0.180	1.040	0.011	0.001	0.210	0.020	0.000	0.020	0.040	0.060	**0.233**
12	W	0.080	0.360	1.260	0.010	0.010	0.170	0.060	0.110	0.140	0.020	0.030	**0.352**
	M	0.040	0.190	1.040	0.010	0.002	0.220	0.020	0.000	0.020	0.030	0.060	**0.234**
13	W	0.080	0.420	1.370	0.010	0.010	0.160	0.070	0.120	0.130	0.010	0.030	**0.373**
	M	0.040	0.170	1.160	0.013	0.001	0.200	0.020	0.000	0.010	0.030	0.060	**0.251**
14	W	0.090	0.430	1.340	0.020	0.010	0.160	0.070	0.120	0.140	0.010	0.030	**0.379**
	M	0.040	0.170	1.060	0.010	0.001	0.020	0.020	0.000	0.020	0.030	0.060	**0.224**
15	W	0.080	0.410	1.360	0.020	0.010	0.150	0.060	0.130	0.140	0.000	0.020	**0.372**
	M	0.040	0.170	1.020	0.012	0.001	0.020	0.020	0.000	0.020	0.030	0.060	**0.217**
16	W	0.080	0.430	1.380	0.020	0.010	0.140	0.070	0.160	0.130	0.000	0.020	**0.383**
	M	0.040	0.180	1.030	0.011	0.001	0.220	0.020	0.000	0.020	0.030	0.060	**0.232**
17	W	0.070	0.410	1.370	0.020	0.010	0.130	0.060	0.170	0.140	0.000	0.020	**0.372**
	M	0.040	0.180	1.040	0.013	0.001	0.220	0.020	0.000	0.010	0.040	0.060	**0.233**
18	W	0.100	0.480	1.400	0.020	0.000	0.140	0.080	0.170	0.080	0.000	0.010	**0.407**
	M	0.040	0.180	1.050	0.011	0.001	0.240	0.020	0.000	0.010	0.040	0.060	**0.236**
19	W	0.080	0.350	1.280	0.010	0.010	0.160	0.070	0.110	0.140	0.020	0.030	**0.356**
	M	0.040	0.190	1.040	0.013	0.002	0.220	0.020	0.000	0.010	0.040	0.050	**0.233**
20	W	0.080	0.340	1.250	0.010	0.010	0.160	0.070	0.110	0.130	0.020	0.030	**0.351**
	M	0.040	0.190	1.040	0.011	0.002	0.220	0.020	0.000	0.010	0.040	0.060	**0.233**
21	W	0.060	0.240	1.210	0.010	0.000	0.190	0.050	0.100	0.140	0.040	0.050	**0.320**
	M	0.040	0.210	1.040	0.010	0.001	0.220	0.020	0.000	0.010	0.030	0.060	**0.233**
22	W	0.060	0.310	1.270	0.010	0.010	0.160	0.060	0.110	0.140	0.020	0.030	**0.333**
	M	0.040	0.170	1.040	0.009	0.001	0.220	0.020	0.000	0.020	0.040	0.060	**0.234**
23	W	0.080	0.370	1.290	0.010	0.010	0.160	0.080	0.110	0.140	0.020	0.030	**0.360**
	M	0.040	0.190	1.030	0.009	0.000	0.210	0.020	0.000	0.020	0.030	0.060	**0.231**
24	W	0.080	0.380	1.300	0.010	0.010	0.160	0.070	0.110	0.140	0.020	0.030	**0.360**
	M	0.040	0.180	1.050	0.011	0.001	0.220	0.020	0.000	0.020	0.030	0.060	**0.235**
25	W	0.080	0.370	1.340	0.020	0.010	0.150	0.060	0.110	0.140	0.010	0.030	**0.364**
	M	0.040	0.180	1.050	0.011	0.001	0.220	0.020	0.000	0.020	0.030	0.060	**0.235**
26	W	0.080	0.380	1.320	0.020	0.010	0.140	0.070	0.120	0.130	0.010	0.030	**0.363**
	M	0.040	0.190	1.040	0.011	0.002	0.220	0.020	0.000	0.010	0.040	0.060	**0.233**
27	W	0.080	0.410	1.320	0.020	0.010	0.140	0.070	0.130	0.140	0.010	0.020	**0.367**
	M	0.040	0.210	1.040	0.010	0.001	0.220	0.020	0.000	0.010	0.030	0.060	**0.233**